Journal of the Mechanics and Physics of Solids 58 (2010) 1374–1396

Contents lists available at ScienceDirect

Journal of the Mechanics and Physics of Solids

journal homepage: www.elsevier.com/locate/jmps

Analytical modeling of fluid loaded orthogonally rib-stiffened sandwich structures: Sound transmission

F.X. Xin, T.J. Lu *

MOE Key Laboratory for Strength and Vibration, School of Aerospace Xi'an Jiaotong University, Xi'an 710049, PR China

ARTICLE INFO

Article history:
Received 12 January 2010
Received in revised form
20 April 2010
Accepted 16 May 2010

Keywords:
Sound transmission
Wave propagation
Vibration
Sandwich structure
Orthogonal rib-stiffeners

ABSTRACT

An analytic model is developed to investigate the wave propagation and sound transmission characteristics of an infinite sandwich structure reinforced by two sets of orthogonal rib-stiffeners when subjected to convective fluid-loaded pressure. The rib-stiffeners are assumed to be identical and uniformly spaced, which can exert not only tensional forces and bending moments but also torsional moments on the facesheets. Inertial terms of the tensional forces, bending moments and torsional moments are introduced to account for inertial effects arising from the mass of the rib-stiffeners. With the surrounding acoustic fluids restricted by the acoustic wave equation, fluid–structure coupling is considered by imposing velocity continuity condition at fluid–panel interfaces. By applying the Bloch theorem for periodic structures, the structural and acoustic responses are expressed in a superposition form of space harmonics for a given wavenumber. The application of the virtual work principle for one periodic element yields two infinite sets of simultaneous algebraic coupled equations, which are numerically solved by truncating them in a finite range insofar as the solution converges. The validity and feasibility of the analytic model is qualified by comparing model predictions with existing results, in which the necessity and advantage of the exact modeling of rib-stiffener motions are also demonstrated. Specifically, the influences of inertial effects arising from rib-stiffener mass, the periodicity spacing of rib-stiffeners, and the airborne as well as structure-borne paths on the transmission of sound across the sandwich structure are quantified and conclusions of significant practical implications are drawn.

1. Introduction

Lightweight sandwich structures consisting of two parallel plates (as the facesheets) reinforced by sets of spatially periodic rib-stiffeners (as the core) form a class of structural elements of practical importance in a wide range of engineering applications, such as aircraft fuselages and ship/submarine hulls (Dozio and Ricciardi, 2009; Fahy and Lindqvist, 1976; Langley et al., 1997; Lee and Kim, 2002; Mace, 1981, 1996; Mead and Yaman, 1991; Xin and Lu, submitted for publication). Typically, these periodic rib-stiffeners construct identical and uniformly spaced sets having a repetitive structural geometry in either one- or two-dimensions. Since aerospace and marine vehicles are usually subjected to sound excitation and/or dynamic impact (Graham, 1995; Hambric et al., 2004; Lucey, 1998; Maury et al., 2001; Xin et al., 2009b), the wave propagation and acoustic characteristics of these periodic structures become increasingly important for

* Corresponding author. Tel.: +86 29 82665600; fax: +86 29 83234781.
E-mail addresses: fengxian.xin@gmail.com (F.X. Xin), tjlu@mail.xjtu.edu.cn (T.J. Lu).

0022-5096/$ - see front matter © 2010 Elsevier Ltd. All rights reserved.
doi:10.1016/j.jmps.2010.05.008

predicting the internal and external sound pressure levels. When the wavelength of flexural wave in the periodically rib-stiffened structure is much greater than stiffener separation, the structure can be approximately regarded as an orthotropic plate. At relatively high frequencies, the wavelength is on the same order as the stiffener separation, and hence the spatially periodic rib-stiffeners should be modeled exactly to comprehend the dynamic and acoustic characteristics of the structure as a whole (Lee and Kim, 2002; Mace, 1980a, b, 1996; Xin and Lu, submitted for publication). The aim is to formulate a physically based analytic model of desirable accuracy for the vibroacoustic response of the sandwich structure, which can in due course be employed in conjunction with optimization techniques to design more effective lightweight soundproofing structures.

A rich literature (e.g., Fahy and Lindqvist, 1976; Lee and Kim, 2002; Mead, 1970, 1996; Mead and Mallik, 1976; Mead and Pujara, 1971; Mead and Yaman, 1991; Rao and Mallik, 1977; Ruzzene, 2004; Spadoni and Ruzzene, 2006; Yin et al., 2007) exists on the theoretical modeling and analysis of wave propagation and dynamic performance of periodically rib-stiffened beams and plates. Focusing on free wave propagation in periodically supported, infinite beams, Mead (1970) found that a freely propagating flexural wave in such a beam must be regarded as a wave group, having components of different wavelengths, phase velocities and directions. A mechanism of whereby slow, subsonic convected pressure fields can generate supersonic, radiating flexural waves was also elucidated. A detailed literature review was reported by Mead (1996) on wave propagation in continuous periodic structures contributed by the Southampton University from 1964 to 1995. More recently, using the transfer matrix approach, Liu and Bhattacharya (2009) obtained dispersion relations for elastic waves propagating in sandwich structures. Ichchou et al. (2008a, b) addressed the issue of energy propagation in a ribbed plate by analyzing its response in the wavenumber space, and derived dispersion relationships between the wavenumber and frequency. Li and Wang (2005), Li et al. (2005) and Wang et al. (2008) performed comprehensive studies on localization of elastic waves in disordered periodic structures, with the underlying mechanism of wave decay phenomenon in such structures revealed. It should be pointed out that the aforementioned contributions on wave propagation and dynamic response of structures are not meant to be exhaustive, whilst a few other specialized topics such as the localized waves in disorder structures, turbulent boundary layer excited vibrations, and fluttering of aircraft wings are beyond the scope of the present research.

Existing studies on the vibroacoustic response of periodic structures may be grouped into two main categories: sound radiation under point loading (Leppington et al., 1984, 1986) and sound transmission due to convective fluid-loaded pressure excitation (Cooper and Crighton, 1998a, b; Crighton, 1984; Leppington, 1989; Leppington et al., 2002, 1987). Particularly, for periodically rib-stiffened structures, two approaches have been used to deal with the relevant issues. Firstly, the technique of Fourier transform was often employed (Lin and Garrelick, 1977; Mace, 1980a–c, 1981, 1996; Maxit, 2009; Rumerman, 1975; Takahashi, 1983; Yin et al., 2007). For example, Rumerman (1975) presented a general solution for the forced vibration of an infinite thin plate, periodically stiffened by identical, uniform ribs, with the forces and bending moments of the ribs considered via the impedances of the ribs and plate. However, the torsional moments and inertial effects of the ribs were not included in the analysis, and no numerical results were given. Mace (1980c) analyzed sound radiation from a point-excited infinite fluid-loaded plate reinforced by two sets of parallel stiffeners; however, the moments of the rib-stiffeners were again ignored. Considering only the forces of rib-stiffeners, Mace (1981) also studied the radiation of sound from a two-dimensional (2D) plate reinforced with two sets of orthogonal line stiffeners under fluid-loaded harmonic incident pressure. Recently, from the viewpoint of vibroacoustic response in wavenumber space, Maxit (2009) proposed an efficient method based on the Fourier transform technique to estimate the vibration and sound radiation from a stiffened fluid-loaded plate excited by a mechanical point force.

Secondly, it has been established that the space-harmonic approach evolving from the consideration of progressive wave propagation is also well suited for studying the vibroacoustic response of periodically rib-stiffened structures (Lee and Kim, 2002; Legault and Atalla, 2009; Mead, 1970, 1996; Mead and Pujara, 1971; Wang et al., 2005; Xin and Lu, in press; Xin et al., 2008a). For instance, the response of periodically supported beams to convected random loading was evaluated by Mead and Pujara (1971) in terms of space harmonic series: only as few as three terms were required to obtain a solution of acceptable accuracy in comparison with the exact solution. The same approach was adopted by Lee and Kim (2002) to study the sound transmission characteristics of a thin plate reinforced by equally spaced line stiffeners, with parametric studies conducted to provide guidelines for the practical design of the system. Extending this approach to parallelly rib-stiffened sandwich structure, Wang et al. (2005) developed an deterministic analytical model by coupling the acoustic and structural vibrations and then employing the virtual work principle. However, the model does not provide a complete description of the motions of the rib-stiffeners and their interaction with the face panels, as only tensional forces and bending moments are considered. A refined theoretical model of Wang et al. (2005) was proposed by Legault and Atalla (2009) to investigate the transmission of sound through a typical aircraft sidewall panel, i.e., sandwich structure reinforced by parallel rib-stiffeners, with fiberglass filled in the cavity: again, only the tensional forces and bending moments of the rib-stiffeners are included.

While previous researches focused mainly on relatively simple sandwich constructions and approximated the rib-stiffeners as an Euler-beam or a combination of translational spring and rotational spring, an exact theoretical model concerning the vibroacoustic response of more complex structures (e.g., two-dimensional sandwich structures orthogonally reinforced by periodic rib-stiffeners) is desirable. In addition to helping exploring the underlying physical subtleties, the model should also serve as benchmark checking for approximate analytical approaches, with a small computational expense afforded compared to numerical methods such as the finite element method (FEM) and the

boundary element method (BEM). With focus placed on 2D sandwich structures reinforced orthogonally with periodic rib-stiffeners under point force excitations, Xin and Lu (submitted for publication) developed such an exact model for their sound radiation characteristics using the Fourier transform technique.

Built upon the work of Xin and Lu (submitted for publication), the physical process of sound transmission through an infinite orthogonally rib-stiffened sandwich structure subjected to convective harmonic fluid-loaded pressure is analytically formulated and solved by employing the space harmonic approach. All possible motions of the rib-stiffeners are included by introducing the tensional forces, bending moments and torsional moments as well as the corresponding inertial terms into the governing equations of the two face panels. Furthermore, the surrounding acoustic fluids are restricted by the acoustic wave equation, and fluid–structure coupling is incorporated by enforcing velocity continuity conditions at fluid–panel interfaces. For one periodic element, applying the principle of virtual work yields two infinite sets of simultaneous algebraic coupled equations, which are numerically solved by truncating them in a finite range insofar as the solution converges. For validation, the predictions of the present analytic model are compared with previous published results, with good overall agreement achieved. Moreover, the necessity and advantage of modeling exactly the motions of the orthogonal rib-stiffeners are also affirmed by comparing the complete model with its simplified version as well as the model of Wang et al. (2005). In the perspective of both physical understanding and practical structural design, the dependence of sound transmission of the structure upon the inertial effects arising from rib-stiffener mass, the airborne and structure-borne paths, and the periodicity spacings of rib-stiffeners is systematically studied and conclusions of referential significance deduced.

2. Vibroacoustic response to convective harmonic fluid-loaded pressure

2.1. Description of the problem

Consider two infinite parallel face panels reinforced by two periodic sets of orthogonal rib-stiffeners having periodic uniform spacings l_x and l_y in the x- and y-directions, respectively (see Fig. 1). A right-handed Cartesian co-ordinate system (x,y,z) is established, with its x- and y-axis positioned separately along one pair of the orthogonal rib-stiffeners and the positive direction of the z-axis pointing downward (Fig. 1). The upper panel located at $z=0$ and the bottom panel located at $z=h_1+d$ separate the acoustic fluid in the spatial field into three parts: the upper field occupying the half-space $z<0$, the middle field filling the space $h_1<z<h_1+d$ (i.e., in between the two panels and divided periodically by the rib-stiffeners), and the lower field occupying the other half-space $z>h_1+h_2+d$. Both the upper panel (thickness h_1) and the bottom panel (thickness h_2) are modeled as Kirchhoff thin plates. Let t_x and t_y denote separately the thickness of the x- and y-wise rib-stiffeners.

An oblique plane sound wave $p(\mathbf{r},t)$ varying harmonically in time is incident upon the upper panel of the sandwich structure with elevation angle φ and azimuth angle θ. Consequently, a distributed load induced by the incident sound pressure wave is exerting on the panel, which in turn induces a bending wave that propagates along the panel. The bending wave in the upper panel is transmitted to the bottom panel via two paths, namely, the structure-borne path (i.e., the orthogonal rib-stiffeners) and the airborne path (i.e., the air constrained in between the two panels). The transmitted bending wave in the bottom panel radiates sound pressure wave into the semi-infinite acoustic fluid in contact with the bottom panel (see Fig. 1(b)). The analytic model to be developed below not only tackles exactly with the physical process of sound transmission through the sandwich structure, but also accounts for the air–structure coupling. Both the acoustic fluid constrained in between the two panels ($h_1<z<h_1+d$) and the semi-infinite fluids in contact with the upper panel ($z<0$) and the bottom panel ($z>h_1+h_2+d$) satisfy the wave equation. Furthermore, the tensional, bending and torsional motions of the rib-stiffeners and their corresponding inertial effects are all taken into account in the proposed model.

2.2. Analytic formulation of panel vibration and sound transmission

Given the periodic nature of the orthogonal rib-stiffened sandwich structure, the Bloch or Floquet theorem (Brillouin, 1953) is utilized here to express the panel vibration, which is well suitable to address wave propagation and vibration issues of periodic structures (Wang et al., 2009a, b, 2010). The displacements $w(x, y)$ of such a system at corresponding points in different periodic elements are related by a spatial periodic function (i.e., a bay-to-bay multiplicative factor, linking the motion of corresponding points in adjacent bays), as

$$w(x+ml_x,y+nl_y)=w(x,y)e^{-ik_xml_x}e^{-ik_ynl_y} \tag{1}$$

Therefore, it is convenient to express the motion of each panel as a summation of one set of space harmonic series. For a 2D sandwich structure stiffened by identical ribs which repeat in the x- and y-directions and excited by a harmonic plane sound wave (i.e., the convective fluid-loaded pressure) $p(x,y,z;t)=Ie^{-i(k_xx+k_yy+k_zz-\omega t)}$, the panel responses $w_j(x,y;t)$ ($j=1, 2$ for the upper and bottom panel, respectively) can be expressed using space harmonic expansion (Mace, 1981; Mead and Pujara, 1971; Xin et al., 2010), as

$$w_1(x,y;t)=\sum_{m=-\infty}^{+\infty}\sum_{n=-\infty}^{+\infty}\alpha_{1,mn}e^{-i[(k_x+2m\pi/l_x)x+(k_y+2n\pi/l_y)y-\omega t]} \tag{2}$$

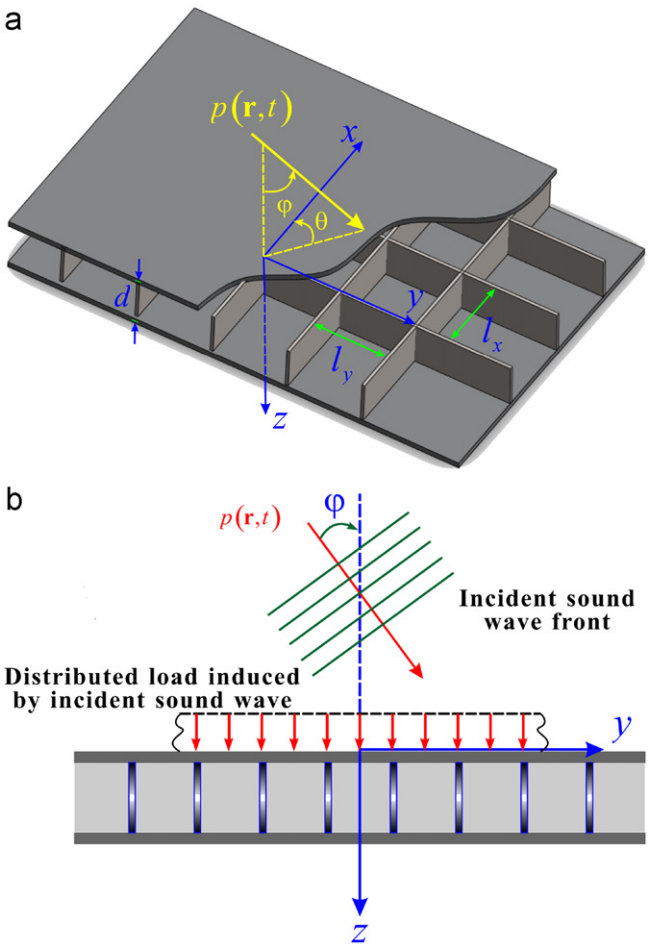

Fig. 1. Schematic illustration of an orthogonally rib-stiffened sandwich subjected to incident sound pressure wave: (a) global view and (b) side view of (a).

$$w_2(x,y;t)=\sum_{m=-\infty}^{+\infty}\sum_{n=-\infty}^{+\infty}\alpha_{2,mn}\,e^{-i[(k_x+2m\pi/l_x)x+(k_y+2n\pi/l_y)y-\omega t]} \tag{3}$$

where the (m, n)th harmonic wave components in the two panels have the same wavenumbers $(k_x+2m\pi/l_x,\ k_y+2n\pi/l_y)$ but different amplitudes, i.e.,

$$\alpha_{1,mn}=\frac{1}{l_x l_y}\int_0^{l_x}\int_0^{l_y} w_1(x,y;t)\,e^{i[(k_x+2m\pi/l_x)x+(k_y+2n\pi/l_y)y-\omega t]}\,dx\,dy \tag{4}$$

$$\alpha_{2,mn}=\frac{1}{l_x l_y}\int_0^{l_x}\int_0^{l_y} w_2(x,y;t)\,e^{i[(k_x+2m\pi/l_x)x+(k_y+2n\pi/l_y)y-\omega t]}\,dx\,dy \tag{5}$$

In Eqs. (2) and (3), the terms with $k_x+2m\pi/l_x>0$ (or $k_y+2n\pi/l_y>0$) stand for positive-going harmonic waves in the x-direction (or the y-direction) and those with $k_x+2m\pi/l_x<0$ (or $k_y+2n\pi/l_y<0$) denote negative-going harmonic waves in the x-direction (or the y-direction).

When sound pressure $p(\mathbf{r},t)=Ie^{-i(\mathbf{k}\cdot\mathbf{r}-\omega t)}$ is incident on the upper panel, the incident sound partly reflected at the air–panel interface and the radiated sound by the vibrating panel constitute the negative-going waves in the upper semi-infinite acoustic fluid domain. The positive-going wave (i.e., the incident sound wave) and the negative-going wave (i.e., the reflected plus radiated sound waves) compose the resultant sound pressure imposed on the upper panel, which are transmitted through the sandwich structure into the semi-infinite space adjacent to the bottom panel, creating thence the transmitted sound pressure. Therefore, sound pressure in the upper semi-infinite field can be expressed as (Xin et al., 2010)

$$P_1(x,y,z;t)=Ie^{-i(k_x x+k_y y+k_z z-\omega t)}+\sum_{m=-\infty}^{+\infty}\sum_{n=-\infty}^{+\infty}\beta_{mn}\,e^{-i[(k_x+2m\pi/l_x)x+(k_y+2n\pi/l_y)y-k_{z,mn}z-\omega t]} \tag{6}$$

Similarly, sound pressure in the middle field in between the two panels are expressed by space harmonic series as

$$P_2(x,y,z;t)=\sum_{m=-\infty}^{+\infty}\sum_{n=-\infty}^{+\infty}\varepsilon_{mn}\,e^{-i\left[(k_x+2m\pi/l_x)x+(k_y+2n\pi/l_y)y+k_{z,mn}z-\omega t\right]} + \sum_{m=-\infty}^{+\infty}\sum_{n=-\infty}^{+\infty}\zeta_{mn}\,e^{-i\left[(k_x+2m\pi/l_x)x+(k_y+2n\pi/l_y)y-k_{z,mn}z-\omega t\right]} \tag{7}$$

The transmitted sound pressure in the bottom semi-infinite field only consists of positive-going wave:

$$P_3(x,y,z;t)=\sum_{m=-\infty}^{+\infty}\sum_{n=-\infty}^{+\infty}\xi_{mn}\,e^{-i\left[(k_x+2m\pi/l_x)x+(k_y+2n\pi/l_y)y+k_{z,mn}z-\omega t\right]} \tag{8}$$

In the above expressions, I is the amplitude of incident sound pressure, β_{mn} and ζ_{mn} are the (m, n)th space harmonic amplitude of negative-going wave in the incident field and in the middle field, respectively, ε_{mn} and ξ_{mn} are the (m, n)th space harmonic amplitude of positive-going wave in the middle field and in the transmitted field, respectively. The wavenumber components in the x-, y- and z-directions are determined by the elevation angle and azimuth angle of the incident sound wave, as

$$k_x=k_0\sin\varphi\cos\theta,\quad k_y=k_0\sin\varphi\sin\theta,\quad k_z=k_0\cos\varphi \tag{9}$$

where $k_{z,mn}$ is the (m, n)th space harmonic wavenumber in the z-direction which, upon applying the Helmholtz equation, is given by

$$k_{z,mn}=\sqrt{\left(\frac{\omega}{c_0}\right)^2-\left(k_x+\frac{2m\pi}{l_x}\right)^2-\left(k_y+\frac{2n\pi}{l_y}\right)^2} \tag{10}$$

Note that, when $(\omega/c_0)^2<(k_x+2m\pi/l_x)^2+(k_y+2n\pi/l_y)^2$, the pressure waves become evanescent waves (Wang et al., 2005; Xin and Lu, in press; Xin et al., 2008a) so that $k_{z,mn}$ should be taken as

$$k_{z,mn}=i\sqrt{\left(k_x+\frac{2m\pi}{l_x}\right)^2+\left(k_y+\frac{2n\pi}{l_y}\right)^2-\left(\frac{\omega}{c_0}\right)^2} \tag{11}$$

The two orthogonal sets of rib-stiffeners uniformly distributed in between the two face panels impose a strong constraint on the motions of the panels, which constitute the structure-borne path for sound transmission and wave propagation. To model accurately the vibroacoustic behavior of the sandwich, the dynamic motions of the rib-stiffeners should be carefully taken into account, which include tensional, bending and torsional vibrations pertinent to tensional forces, bending moments and torsional moments imposed on the connected panels. To account for the inertial effects of these motions arising from the mass of the rib-stiffeners, the resultant tensional forces, bending and torsional moments acting on the upper and bottom panels are not identical, which are marked here by (Q^+, M^+, M_T^+) and (Q^-, M^-, M_T^-). Fig. 2 illustrates the conventions used for the tensional forces, bending moments and torsional moments at the interface between the upper panel and the x/y-wise rib-stiffeners. The same apply at the interface between the bottom panel and the x/y-wise rib-stiffeners, with (Q^+, M^+, M_T^+) replaced by (Q^-, M^-, M_T^-).

Given that the incident sound pressure wave varies harmonically in time, the dynamic responses of the two face panels are also harmonically dependent upon time. For simplicity, the harmonic time dependence $e^{-i\omega t}$ will be suppressed throughout the paper henceforth.

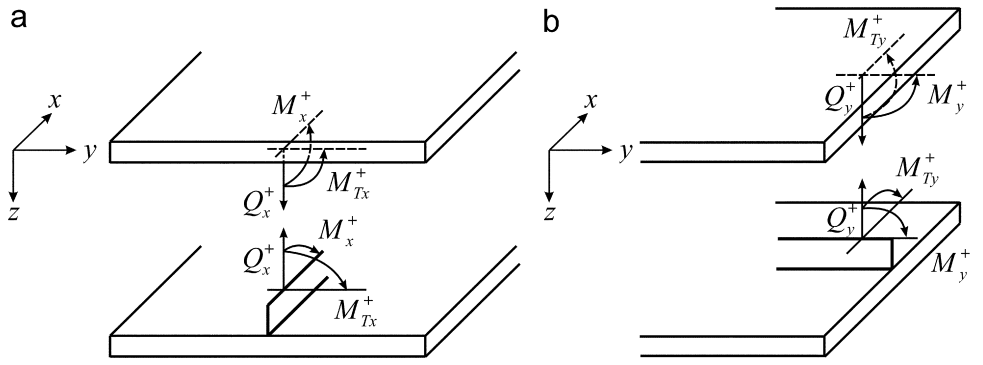

Fig. 2. Conventions for tensional forces, bending moments and torsional moments between the upper panel and (a) x-wise rib-stiffeners and (b) y-wise rib-stiffeners. Similar conventions hold at the interface between the bottom panel and the x/y-wise rib-stiffeners by replacing (Q^+, M^+, M_T^+) with (Q^-, M^-, M_T^-)], which is not shown here for brevity.

The resultant pressure exerted on the upper panel is contributed by the incident sound wave, the negative-going wave on the incident side $P_1(x,y,0)$ and the middle field pressure $P_2(x,y,h_1)$ on the other side. For the bottom panel, the net pressure is a combination of the transmitted sound pressure $P_3(x,y,h_1+h_2+d)$ on the transmitted side and the middle field pressure $P_2(x,y,h_1+d)$ on the other side. Under the prescribed Cartesian co-ordinate system, with the tensional forces, bending moments and torsional moments of the rib-stiffeners accounted for, the governing equations for panel vibrations are given by

$$D_1\nabla^4 w_1+m_1\frac{\partial^2 w_1}{\partial t^2}=\sum_{m=-\infty}^{+\infty}\left[Q_y^+\delta(x-ml_x)+\frac{\partial}{\partial y}\left\{M_y^+\delta(x-ml_x)\right\}+\frac{\partial}{\partial x}\left\{M_{Ty}^+\delta(x-ml_x)\right\}\right]$$
$$+\sum_{n=-\infty}^{+\infty}\left[Q_x^+\delta(y-nl_y)+\frac{\partial}{\partial x}\left\{M_x^+\delta(y-nl_y)\right\}+\frac{\partial}{\partial y}\left\{M_{Tx}^+\delta(y-nl_y)\right\}\right]+P_1(x,y,0)-P_2(x,y,h_1) \tag{12}$$

$$D_2\nabla^4 w_2+m_2\frac{\partial^2 w_2}{\partial t^2}=-\sum_{m=-\infty}^{+\infty}\left[Q_y^-\delta(x-ml_x)+\frac{\partial}{\partial y}\left\{M_y^-\delta(x-ml_x)\right\}+\frac{\partial}{\partial x}\left\{M_{Ty}^-\delta(x-ml_x)\right\}\right]$$
$$-\sum_{n=-\infty}^{+\infty}\left[Q_x^-\delta(y-nl_y)+\frac{\partial}{\partial x}\left\{M_x^-\delta(y-nl_y)\right\}+\frac{\partial}{\partial y}\left\{M_{Tx}^-\delta(y-nl_y)\right\}\right]+P_2(x,y,h_1+d)-P_3(x,y,h_1+h_2+d) \tag{13}$$

where $\nabla^4=(\partial^2/\partial x^2+\partial^2/\partial y^2)^2$, (w_1, w_2), (m_1, m_2) and (D_1, D_2) are the displacements, mass density per unit area and flexural rigidity of the upper and bottom panel, respectively, and $\delta(\cdot)$ is the Dirac delta function.

Since the inertial effects (i.e., inertial tensional forces, inertial bending moments and inertial torsional moments) of the rib-stiffeners have been taken into account, the factual tensional forces Q, bending moments M and torsional moments M_T imposed on the two face panels are unequal. Therefore, as shown in Fig. 2, superscripts + and − associated separately with the upper and bottom panels are introduced to differentiate this discrepancy, with subscripts x and y introduced to signify the terms arising from the x- and y-wise rib-stiffeners, respectively.

Taking the inertial effects of the rib-stiffeners into consideration, and applying the Hooke's law and the Newton's second law, one can express the tensional forces of the rib-stiffeners as (Xin and Lu, submitted for publication)

$$Q_x^+=-\frac{K_x(K_x-m_x\omega^2)}{2K_x-m_x\omega^2}w_1+\frac{K_x^2}{2K_x-m_x\omega^2}w_2 \tag{14}$$

$$Q_x^-=-\frac{K_x^2}{2K_x-m_x\omega^2}w_1+\frac{K_x(K_x-m_x\omega^2)}{2K_x-m_x\omega^2}w_2 \tag{15}$$

$$Q_y^+=-\frac{K_y(K_y-m_y\omega^2)}{2K_y-m_y\omega^2}w_1+\frac{K_y^2}{2K_y-m_y\omega^2}w_2 \tag{16}$$

$$Q_y^-=-\frac{K_y^2}{2K_y-m_y\omega^2}w_1+\frac{K_y(K_y-m_y\omega^2)}{2K_y-m_y\omega^2}w_2 \tag{17}$$

where ω is the circular frequency, (K_x, K_y) are the tensional stiffness of half rib-stiffeners per unit length and (m_x, m_y) are the line mass density of the x- and y-wise rib-stiffeners, respectively.

Similarly, the bending moments of the rib-stiffeners can be expressed as (Xin and Lu, submitted for publication)

$$M_x^+=\frac{E_xI_x^*(E_xI_x^*-\rho_xI_x\omega^2)}{2E_xI_x^*-\rho_xI_x\omega^2}\frac{\partial^2 w_1}{\partial x^2}-\frac{E_x^2I_x^{*2}}{2E_xI_x^*-\rho_xI_x\omega^2}\frac{\partial^2 w_2}{\partial x^2} \tag{18}$$

$$M_x^-=\frac{E_x^2I_x^{*2}}{2E_xI_x^*-\rho_xI_x\omega^2}\frac{\partial^2 w_1}{\partial x^2}-\frac{E_xI_x^*(E_xI_x^*-\rho_xI_x\omega^2)}{2E_xI_x^*-\rho_xI_x\omega^2}\frac{\partial^2 w_2}{\partial x^2} \tag{19}$$

$$M_y^+=\frac{E_yI_y^*(E_yI_y^*-\rho_yI_y\omega^2)}{2E_yI_y^*-\rho_yI_y\omega^2}\frac{\partial^2 w_1}{\partial y^2}-\frac{E_y^2I_y^{*2}}{2E_yI_y^*-\rho_yI_y\omega^2}\frac{\partial^2 w_2}{\partial y^2} \tag{20}$$

$$M_y^-=\frac{E_y^2I_y^{*2}}{2E_yI_y^*-\rho_yI_y\omega^2}\frac{\partial^2 w_1}{\partial y^2}-\frac{E_yI_y^*(E_yI_y^*-\rho_yI_y\omega^2)}{2E_yI_y^*-\rho_yI_y\omega^2}\frac{\partial^2 w_2}{\partial y^2} \tag{21}$$

where $(E_xI_x^*, E_yI_y^*)$ are the bending stiffness of half rib-stiffeners per unit length, and (ρ_x, ρ_y), (I_x, I_y) are the mass density and polar moment of inertia for the rib-stiffeners, with subscripts x and y indicating the corresponding orientations of the rib-stiffeners.

Following the same procedures, the torsional moments of the rib-stiffeners are given by (Xin and Lu, submitted for publication)

$$M_{Tx}^{+}=\frac{G_xJ_x^*(G_xJ_x^*-\rho_xJ_x\omega^2)}{2G_xJ_x^*-\rho_xJ_x\omega^2}\frac{\partial^2 w_1}{\partial x\partial y}-\frac{G_x^2J_x^{*2}}{2G_xJ_x^*-\rho_xJ_x\omega^2}\frac{\partial^2 w_2}{\partial x\partial y} \tag{22}$$

$$M_{Tx}^{-}=\frac{G_x^2J_x^{*2}}{2G_xJ_x^*-\rho_xJ_x\omega^2}\frac{\partial^2 w_1}{\partial x\partial y}-\frac{G_xJ_x^*(G_xJ_x^*-\rho_xJ_x\omega^2)}{2G_xJ_x^*-\rho_xJ_x\omega^2}\frac{\partial^2 w_2}{\partial x\partial y} \tag{23}$$

$$M_{Ty}^{+}=\frac{G_yJ_y^*(G_yJ_y^*-\rho_yJ_y\omega^2)}{2G_yJ_y^*-\rho_yJ_y\omega^2}\frac{\partial^2 w_1}{\partial y\partial x}-\frac{G_y^2J_y^{*2}}{2G_yJ_y^*-\rho_yJ_y\omega^2}\frac{\partial^2 w_2}{\partial y\partial x} \tag{24}$$

$$M_{Ty}^{-}=\frac{G_y^2J_y^{*2}}{2G_yJ_y^*-\rho_yJ_y\omega^2}\frac{\partial^2 w_1}{\partial y\partial x}-\frac{G_yJ_y^*(G_yJ_y^*-\rho_yJ_y\omega^2)}{2G_yJ_y^*-\rho_yJ_y\omega^2}\frac{\partial^2 w_2}{\partial y\partial x} \tag{25}$$

where $(G_xJ_x^*,\ G_yJ_y^*)$ are the torsional stiffness of half rib-stiffeners per unit length, and (J_x, J_y) are the torsional moments of inertia of the rib-stiffeners.

In the above expressions for the tensional forces, bending moments and torsional moments, the geometrical properties of rib-stiffener cross-sections are given by

$$K_x=\frac{E_xt_x}{d/2},\quad K_y=\frac{E_yt_y}{d/2} \tag{26}$$

$$I_x^*=\frac{t_x(d/2)^3}{12},\quad I_y^*=\frac{t_y(d/2)^3}{12},\quad I_x=\frac{t_xd^3}{12},\quad I_y=\frac{t_yd^3}{12} \tag{27}$$

$$J_x^*=\frac{t_x^3d}{2}\left[\frac{1}{3}-\frac{64}{\pi^5}\frac{2t_x}{d}\sum_{n=1,3,5,\ldots}^{\infty}\frac{\tanh(n\pi d/4t_x)}{n^5}\right] \tag{28}$$

$$J_y^*=\frac{t_y^3d}{2}\left[\frac{1}{3}-\frac{64}{\pi^5}\frac{2t_y}{d}\sum_{n=1,3,5,\ldots}^{\infty}\frac{\tanh(n\pi d/4t_y)}{n^5}\right] \tag{29}$$

$$J_x=t_x^3d\left[\frac{1}{3}-\frac{64}{\pi^5}\frac{t_x}{d}\sum_{n=1,3,5,\ldots}^{\infty}\frac{\tanh(n\pi d/2t_x)}{n^5}\right] \tag{30}$$

$$J_y=t_y^3d\left[\frac{1}{3}-\frac{64}{\pi^5}\frac{t_y}{d}\sum_{n=1,3,5,\ldots}^{\infty}\frac{\tanh(n\pi d/2t_y)}{n^5}\right] \tag{31}$$

To simplify Eqs. (14)–(25), the following sets of specified characteristics are utilized to replace the coefficients of the general displacements:

(1) Replacement of tensional force coefficients

$$R_{Q1}=\frac{K_x(K_x-m_x\omega^2)}{2K_x-m_x\omega^2},\quad R_{Q2}=\frac{K_x^2}{2K_x-m_x\omega^2} \tag{32}$$

$$R_{Q3}=\frac{K_y(K_y-m_y\omega^2)}{2K_y-m_y\omega^2},\quad R_{Q4}=\frac{K_y^2}{2K_y-m_y\omega^2} \tag{33}$$

(2) Replacement of bending moment coefficients

$$R_{M1}=\frac{E_xI_x^*(E_xI_x^*-\rho_xI_x\omega^2)}{2E_xI_x^*-\rho_xI_x\omega^2},\quad R_{M2}=\frac{E_x^2I_x^{*2}}{2E_xI_x^*-\rho_xI_x\omega^2} \tag{34}$$

$$R_{M3}=\frac{E_yI_y^*(E_yI_y^*-\rho_yI_y\omega^2)}{2E_yI_y^*-\rho_yI_y\omega^2},\quad R_{M4}=\frac{E_y^2I_y^{*2}}{2E_yI_y^*-\rho_yI_y\omega^2} \tag{35}$$

(3) Replacement of torsional moment coefficients

$$R_{T1}=\frac{G_xJ_x^*(G_xJ_x^*-\rho_xJ_x\omega^2)}{2G_xJ_x^*-\rho_xJ_x\omega^2},\quad R_{T2}=\frac{G_x^2J_x^{*2}}{2G_xJ_x^*-\rho_xJ_x\omega^2} \tag{36}$$

$$R_{T3}=\frac{G_yJ_y^*(G_yJ_y^*-\rho_yJ_y\omega^2)}{2G_yJ_y^*-\rho_yJ_y\omega^2},\quad R_{T4}=\frac{G_y^2J_y^{*2}}{2G_yJ_y^*-\rho_yJ_y\omega^2} \tag{37}$$

Adopting Eqs. (32)–(37) and substituting Eqs. (2) and (3) into Eqs. (14)–(25), we can simplify the expressions of the tensional forces, bending moments and torsional moments, as follows:

(1) Tensional forces

$$Q_x^+ = \sum_{m=-\infty}^{+\infty}\sum_{n=-\infty}^{+\infty}(-R_{Q1}\alpha_{1,mn}+R_{Q2}\alpha_{2,mn})e^{-i[(k_x+2m\pi/l_x)x+(k_y+2n\pi/l_y)y]} \tag{38}$$

$$Q_x^- = \sum_{m=-\infty}^{+\infty}\sum_{n=-\infty}^{+\infty}(-R_{Q2}\alpha_{1,mn}+R_{Q1}\alpha_{2,mn})e^{-i[(k_x+2m\pi/l_x)x+(k_y+2n\pi/l_y)y]} \tag{39}$$

$$Q_y^+ = \sum_{m=-\infty}^{+\infty}\sum_{n=-\infty}^{+\infty}(-R_{Q3}\alpha_{1,mn}+R_{Q4}\alpha_{2,mn})e^{-i[(k_x+2m\pi/l_x)x+(k_y+2n\pi/l_y)y]} \tag{40}$$

$$Q_y^- = \sum_{m=-\infty}^{+\infty}\sum_{n=-\infty}^{+\infty}(-R_{Q4}\alpha_{1,mn}+R_{Q3}\alpha_{2,mn})e^{-i[(k_x+2m\pi/l_x)x+(k_y+2n\pi/l_y)y]} \tag{41}$$

(2) Bending moments

$$M_x^+ = \sum_{m=-\infty}^{+\infty}\sum_{n=-\infty}^{+\infty}(-R_{M1}\alpha_{1,mn}+R_{M2}\alpha_{2,mn})\alpha_m^2 e^{-i[(k_x+2m\pi/l_x)x+(k_y+2n\pi/l_y)y]} \tag{42}$$

$$M_x^- = \sum_{m=-\infty}^{+\infty}\sum_{n=-\infty}^{+\infty}(-R_{M2}\alpha_{1,mn}+R_{M1}\alpha_{2,mn})\alpha_m^2 e^{-i[(k_x+2m\pi/l_x)x+(k_y+2n\pi/l_y)y]} \tag{43}$$

$$M_y^+ = \sum_{m=-\infty}^{+\infty}\sum_{n=-\infty}^{+\infty}(-R_{M3}\alpha_{1,mn}+R_{M4}\alpha_{2,mn})\beta_n^2 e^{-i[(k_x+2m\pi/l_x)x+(k_y+2n\pi/l_y)y]} \tag{44}$$

$$M_y^- = \sum_{m=-\infty}^{+\infty}\sum_{n=-\infty}^{+\infty}(-R_{M4}\alpha_{1,mn}+R_{M3}\alpha_{2,mn})\beta_n^2 e^{-i[(k_x+2m\pi/l_x)x+(k_y+2n\pi/l_y)y]} \tag{45}$$

(3) Torsional moments

$$M_{Tx}^+ = \sum_{m=-\infty}^{+\infty}\sum_{n=-\infty}^{+\infty}(-R_{T1}\alpha_{1,mn}+R_{T2}\alpha_{2,mn})\alpha_m\beta_n e^{-i[(k_x+2m\pi/l_x)x+(k_y+2n\pi/l_y)y]} \tag{46}$$

$$M_{Tx}^- = \sum_{m=-\infty}^{+\infty}\sum_{n=-\infty}^{+\infty}(-R_{T2}\alpha_{1,mn}+R_{T1}\alpha_{2,mn})\alpha_m\beta_n e^{-i[(k_x+2m\pi/l_x)x+(k_y+2n\pi/l_y)y]} \tag{47}$$

$$M_{Ty}^+ = \sum_{m=-\infty}^{+\infty}\sum_{n=-\infty}^{+\infty}(-R_{T3}\alpha_{1,mn}+R_{T4}\alpha_{2,mn})\alpha_m\beta_n e^{-i[(k_x+2m\pi/l_x)x+(k_y+2n\pi/l_y)y]} \tag{48}$$

$$M_{Ty}^- = \sum_{m=-\infty}^{+\infty}\sum_{n=-\infty}^{+\infty}(-R_{T4}\alpha_{1,mn}+R_{T3}\alpha_{2,mn})\alpha_m\beta_n e^{-i[(k_x+2m\pi/l_x)x+(k_y+2n\pi/l_y)y]} \tag{49}$$

2.3. The acoustic pressure and continuity condition

The acoustic pressure $P_1(x,y,z)$ in the incident field, $P_2(x,y,z)$ in the field between the two face panels and $P_3(x,y,z)$ in the transmitted field all satisfy the wave equation (Spadoni and Ruzzene, 2006; Xin and Lu, 2009; Xin et al., 2008b):

$$\left[\frac{\partial^2}{\partial x^2}+\frac{\partial^2}{\partial y^2}+\frac{\partial^2}{\partial z^2}+k_0^2\right]P_i = 0 \quad (i=1,2,3) \tag{50}$$

where k_0 is the wavenumber of the incident sound. The momentum equation is applied to ensure the equality of panel velocity and fluid velocity on the panel surface, i.e., the continuity condition of fluid–structure coupling (Lin and Garrelick, 1977; Xin et al., 2009b):

$$\left.\frac{\partial P_1}{\partial z}\right|_{z=0} = \omega^2\rho_0 w_1, \quad \left.\frac{\partial P_2}{\partial z}\right|_{z=h_1} = \omega^2\rho_0 w_1 \tag{51}$$

$$\frac{\partial P_2}{\partial z}\Big|_{z=h_1+d}=\omega^2\rho_0 w_2,\quad \frac{\partial P_3}{\partial z}\Big|_{z=h_1+h_2+d}=\omega^2\rho_0 w_2 \tag{52}$$

where ρ_0 is the ambient acoustic fluid density. Substitution of Eqs. (2) and (3) as well as Eqs. (6)–(8) into Eqs. (51) and (52) gives rise to

$$-ik_z I e^{-i(k_x x+k_y y)}+\sum_{m=-\infty}^{+\infty}\sum_{n=-\infty}^{+\infty}(ik_{z,mn}\beta_{mn}-\omega^2\rho_0\alpha_{1,mn})e^{-i[(k_x+2m\pi/l_x)x+(k_y+2n\pi/l_y)y]}=0 \tag{53}$$

$$\sum_{m=-\infty}^{+\infty}\sum_{n=-\infty}^{+\infty}\left[ik_{z,mn}(-\varepsilon_{mn}e^{-ik_{z,mn}h_1}+\zeta_{mn}e^{ik_{z,mn}h_1})-\omega^2\rho_0\alpha_{1,mn}\right]e^{-i[(k_x+2m\pi/l_x)x+(k_y+2n\pi/l_y)y]}=0 \tag{54}$$

$$\sum_{m=-\infty}^{+\infty}\sum_{n=-\infty}^{+\infty}\begin{bmatrix}ik_{z,mn}(-\varepsilon_{mn}e^{-ik_{z,mn}(h_1+d)}+\zeta_{mn}e^{ik_{z,mn}(h_1+d)})\\-\omega^2\rho_0\alpha_{2,mn}\end{bmatrix}e^{-i[(k_x+2m\pi/l_x)x+(k_y+2n\pi/l_y)y]}=0 \tag{55}$$

$$\sum_{m=-\infty}^{+\infty}\sum_{n=-\infty}^{+\infty}\left[-ik_{z,mn}\xi_{mn}e^{-ik_{z,mn}(h_1+h_2+d)}-\omega^2\rho_0\alpha_{2,mn}\right]e^{-i[(k_x+2m\pi/l_x)x+(k_y+2n\pi/l_y)y]}=0 \tag{56}$$

Because Eqs. (53)–(56) hold for all possible values of x and y, the relevant coefficients have the following relationships:

$$\beta_{00}=I+\frac{\omega^2\rho_0\alpha_{1,00}}{ik_z} \tag{57}$$

$$\beta_{mn}=\frac{\omega^2\rho_0\alpha_{1,mn}}{ik_{z,mn}},\quad \text{at } m\neq 0||n\neq 0 \tag{58}$$

$$\varepsilon_{mn}=\frac{\omega^2\rho_0\left[\alpha_{1,mn}e^{ik_{z,mn}(h_1+d)}-\alpha_{2,mn}e^{ik_{z,mn}h_1}\right]}{2k_{z,mn}\sin(k_{z,mn}d)} \tag{59}$$

$$\zeta_{mn}=\frac{\omega^2\rho_0\left[\alpha_{1,mn}e^{-ik_{z,mn}(h_1+d)}-\alpha_{2,mn}e^{-ik_{z,mn}h_1}\right]}{2k_{z,mn}\sin(k_{z,mn}d)} \tag{60}$$

$$\xi_{mn}=-\frac{\omega^2\rho_0\alpha_{2,mn}}{ik_{z,mn}}e^{ik_{z,mn}(h_1+h_2+d)} \tag{61}$$

2.4. Solution of the formulations with the virtual work principle

As can be seen from Eqs. (57)–(61), once coefficients $\alpha_{1,mn}$ and $\alpha_{2,mn}$ (i.e., modal amplitudes of the (m, n)th space harmonic flexural waves in the upper and bottom panel, respectively) are determined, coefficients β_{mn}, ε_{mn}, ζ_{mn} and ξ_{mn} are also determined. Coefficients $\alpha_{1,mn}$ and $\alpha_{2,mn}$ can be obtained by solving the system equations derived by applying the principle of virtual work (Lee and Kim, 2002; Mead and Pujara, 1971; Wang et al., 2005). In view of the spatial periodicity of the structure, it is necessary to consider only the virtual work contribution from one period of element (including the attached rib-stiffeners). As the statement of the virtual work principle, the sum of the work done by all the elements in one period of the system must be zero when the system has any one of the virtual displacements:

$$\delta w_j=\delta\alpha_{j,mn}e^{-i[(k_x+2m\pi/l_x)x+(k_y+2n\pi/l_y)y]}\quad (j=1,2) \tag{62}$$

2.4.1. Virtual work of panel elements

The equations governing the vibration responses of the two panel elements in one period of the structure are:

$$D_1\nabla^4 w_1+m_1\frac{\partial^2 w_1}{\partial t^2}-P_1(x,y,0)+P_2(x,y,h_1)=0 \tag{63}$$

$$D_2\nabla^4 w_2+m_2\frac{\partial^2 w_2}{\partial t^2}-P_2(x,y,h_1+d)+P_3(x,y,h_1+h_2+d)=0 \tag{64}$$

The virtual work contributed solely by the panel elements can then be represented as

$$\delta\Pi_{p1}=\int_0^{l_x}\int_0^{l_y}\left[D_1\nabla^4 w_1+m_1\frac{\partial^2 w_1}{\partial t^2}-P_1(x,y,0)+P_2(x,y,h_1)\right]\delta w_1^*\,dx\,dy \tag{65}$$

$$\delta\Pi_{p2}=\int_0^{l_x}\int_0^{l_y}\left[D_2\nabla^4 w_2+m_2\frac{\partial^2 w_2}{\partial t^2}-P_2(x,y,h_1+d)+P_3(x,y,h_1+h_2+d)\right]\delta w_2^*\,dx\,dy \tag{66}$$

where δw_1^* and δw_2^* denote the complex conjugate of the virtual displacement in Eq. (62). Together with Eqs. (2) and (3), (6)–(8) and (57)–(61), Eqs. (65) and (66) can be rewritten in terms of modal amplitudes $\alpha_{1,kl}$ and $\alpha_{2,kl}$, as

$$\delta\Pi_{p1} = = \left\{\left(D_1\left[\left(k_x+\frac{2k\pi}{l_x}\right)^2+\left(k_y+\frac{2l\pi}{l_y}\right)^2\right]^2-m_1\omega^2\right)\alpha_{1,kl}-\frac{\omega^2\rho_0\alpha_{1,kl}}{ik_{z,kl}}+\frac{\omega^2\rho_0\left[\alpha_{1,kl}\cos(k_{z,kl}d)-\alpha_{2,kl}\right]}{k_{z,kl}\sin(k_{z,kl}d)}\right\}l_xl_y\,\delta\alpha_{1,kl}$$
$$-\int_0^{l_x}\int_0^{l_y}2I\,e^{-i(k_xx+k_yy)}\,e^{-i\left[(k_x+2k\pi/l_x)x+(k_y+2l\pi/l_y)y\right]}dx\,dy\,\delta\alpha_{1,kl} \tag{67}$$

$$\delta\Pi_{p2} = = \left\{\left(D_2\left[\left(k_x+\frac{2k\pi}{l_x}\right)^2+\left(k_y+\frac{2l\pi}{l_y}\right)^2\right]^2-m_2\omega^2\right)\alpha_{2,kl}-\frac{\omega^2\rho_0\alpha_{2,kl}}{ik_{z,kl}}-\frac{\omega^2\rho_0\left[\alpha_{1,kl}-\alpha_{2,kl}\cos(k_{z,kl}d)\right]}{k_{z,kl}\sin(k_{z,kl}d)}\right\}l_xl_y\,\delta\alpha_{2,kl} \tag{68}$$

2.4.2. Virtual work of x-wise rib-stiffeners

The virtual work contributions from the tensional forces, bending moments and torsional moments at the interfaces between the x-wise rib-stiffeners (aligned with y=0) with the upper and bottom panels are given by

$$\delta\Pi_{x1} = -\int_0^{l_x}\left[Q_x^+(x,0)+\frac{\partial}{\partial x}M_x^+(x,0)+\frac{\partial}{\partial y}M_{Tx}^+(x,0)\right]\delta\alpha_{1,kl}\,e^{i(k_x+2k\pi/l_x)x}\,dx$$
$$=\sum_{n=-\infty}^{+\infty}\left[R_{Q1}\alpha_{1,kn}-R_{Q2}\alpha_{2,kn}+i\left(k_x+\frac{2k\pi}{l_x}\right)^3(-R_{M1}\alpha_{1,kn}+R_{M2}\alpha_{2,kn})\right.$$
$$\left.+i\left(k_x+\frac{2k\pi}{l_x}\right)\left(k_y+\frac{2l\pi}{l_y}\right)\left(k_y+\frac{2n\pi}{l_y}\right)(-R_{T1}\alpha_{1,kn}+R_{T2}\alpha_{2,kn})\right]l_x\delta\alpha_{1,kl} \tag{69}$$

$$\delta\Pi_{x2} = \int_0^{l_x}\left[Q_x^-(x,0)+\frac{\partial}{\partial x}M_x^-(x,0)+\frac{\partial}{\partial y}M_{Tx}^-(x,0)\right]\delta\alpha_{2,kl}\,e^{i(k_x+2k\pi/l_x)x}\,dx$$
$$=\sum_{n=-\infty}^{+\infty}\left[-R_{Q2}\alpha_{1,kn}+R_{Q1}\alpha_{2,kn}-i\left(k_x+\frac{2k\pi}{l_x}\right)^3(-R_{M2}\alpha_{1,kn}+R_{M1}\alpha_{2,kn})\right.$$
$$\left.-i\left(k_x+\frac{2k\pi}{l_x}\right)\left(k_y+\frac{2l\pi}{l_y}\right)\left(k_y+\frac{2n\pi}{l_y}\right)(-R_{T2}\alpha_{1,kn}+R_{T1}\alpha_{2,kn})\right]l_x\delta\alpha_{2,kl} \tag{70}$$

where $(\partial/\partial y)M_{Tx}^+(x,y=0)=(\partial/\partial y)M_{Tx}^+(x,y)|_{y=0}$ and $(\partial/\partial y)M_{Tx}^-(x,y=0)=(\partial/\partial y)M_{Tx}^-(x,y)|_{y=0}$.

2.4.3. Virtual work of y-wise rib-stiffeners

Likewise, the virtual work contributions from the tensional forces, bending moments and torsional moments at the interfaces between the y-wise rib-stiffeners (aligned with x=0) with the upper and bottom panels are:

$$\delta\Pi_{y1} = -\int_0^{l_y}\left[Q_y^+(0,y)+\frac{\partial}{\partial y}M_y^+(0,y)+\frac{\partial}{\partial x}M_{Ty}^+(0,y)\right]\delta\alpha_{1,kl}\,e^{i(k_y+2l\pi/l_y)y}\,dy$$
$$=\sum_{m=-\infty}^{+\infty}\left[R_{Q3}\alpha_{1,ml}-R_{Q4}\alpha_{2,ml}+i\left(k_y+\frac{2l\pi}{l_y}\right)^3(-R_{M3}\alpha_{1,ml}+R_{M4}\alpha_{2,ml})\right.$$
$$\left.+i\left(k_x+\frac{2k\pi}{l_x}\right)\left(k_x+\frac{2m\pi}{l_x}\right)\left(k_y+\frac{2l\pi}{l_y}\right)(-R_{T3}\alpha_{1,ml}+R_{T4}\alpha_{2,ml})\right]l_y\delta\alpha_{1,kl} \tag{71}$$

$$\delta\Pi_{y2} = \int_0^{l_y}\left[Q_y^-(0,y)+\frac{\partial}{\partial y}M_y^-(0,y)+\frac{\partial}{\partial x}M_{Ty}^-(0,y)\right]\delta\alpha_{2,kl}\,e^{-i(k_y+2l\pi/l_y)y}\,dy$$
$$=\sum_{m=-\infty}^{+\infty}\left[-R_{Q4}\alpha_{1,ml}+R_{Q3}\alpha_{2,ml}-i\left(k_y+\frac{2l\pi}{l_y}\right)^3(-R_{M4}\alpha_{1,ml}+R_{M3}\alpha_{2,ml})\right.$$
$$\left.-i\left(k_x+\frac{2k\pi}{l_x}\right)\left(k_x+\frac{2m\pi}{l_x}\right)\left(k_y+\frac{2l\pi}{l_y}\right)(-R_{T4}\alpha_{1,ml}+R_{T3}\alpha_{2,ml})\right]l_y\delta\alpha_{2,kl} \tag{72}$$

where $(\partial/\partial x)M_{Ty}^+(x=0,y)=(\partial/\partial x)M_{Ty}^+(x,y)|_{x=0}$ and $(\partial/\partial x)M_{Ty}^-(x=0,y)=(\partial/\partial x)M_{Ty}^-(x,y)|_{x=0}$.

2.4.4. Combination of equations

Finally, the virtual work principle requires that

$$\delta\Pi_{p1}+\delta\Pi_{x1}+\delta\Pi_{y1}=0 \tag{73}$$

$$\delta\Pi_{p2}+\delta\Pi_{x2}+\delta\Pi_{y2}=0 \tag{74}$$

Substituting Eqs. (67), (69) and (71) into (73), Eqs. (68), (70) and (72) into (74), and noting that the virtual displacement is arbitrary, we obtain:

$$\begin{aligned}
&\left\{\left[D_1(\alpha_k^2+\beta_l^2)^2-m_1\omega^2\right]\alpha_{1,kl}-\frac{\omega^2\rho_0\alpha_{1,kl}}{ik_{z,kl}}+\frac{\omega^2\rho_0[\alpha_{1,kl}\cos(k_{z,kl}d)-\alpha_{2,kl}]}{k_{z,kl}\sin(k_{z,kl}d)}\right\}l_xl_y\\
&\quad+\sum_{n=-\infty}^{+\infty}\left[R_{Q1}\alpha_{1,kn}-R_{Q2}\alpha_{2,kn}+i\alpha_k(-R_{M1}\alpha_{1,kn}+R_{M2}\alpha_{2,kn})\alpha_k^2+i\beta_l(-R_{T1}\alpha_{1,kn}+R_{T2}\alpha_{2,kn})\alpha_k\beta_n\right]l_x\\
&\quad+\sum_{m=-\infty}^{+\infty}\left[R_{Q3}\alpha_{1,ml}-R_{Q4}\alpha_{2,ml}+i\beta_l(-R_{M3}\alpha_{1,ml}+R_{M4}\alpha_{2,ml})\beta_l^2+i\alpha_k(-R_{T3}\alpha_{1,ml}+R_{T4}\alpha_{2,ml})\alpha_m\beta_l\right]l_y\\
&=\begin{cases}2Il_xl_y & \text{when } k=0\&l=0\\ 0 & \text{when } k\neq0||l\neq0\end{cases}
\end{aligned}\tag{75}$$

$$\begin{aligned}
&\left\{\left[D_2(\alpha_k^2+\beta_l^2)^2-m_2\omega^2\right]\alpha_{2,kl}-\frac{\omega^2\rho_0\alpha_{2,kl}}{ik_{z,kl}}-\frac{\omega^2\rho_0[\alpha_{1,kl}-\alpha_{2,kl}\cos(k_{z,kl}d)]}{k_{z,kl}\sin(k_{z,kl}d)}\right\}l_xl_y\\
&\quad+\sum_{n=-\infty}^{+\infty}\left[-R_{Q2}\alpha_{1,kn}+R_{Q1}\alpha_{2,kn}-i\alpha_k(-R_{M2}\alpha_{1,kn}+R_{M1}\alpha_{2,kn})\alpha_k^2\right]-i\beta_l(-R_{T2}\alpha_{1,kn}+R_{T1}\alpha_{2,kn})\alpha_k\beta_n\Big]l_x\\
&\quad+\sum_{m=-\infty}^{+\infty}\left[-R_{Q4}\alpha_{1,ml}+R_{Q3}\alpha_{2,ml}-i\beta_l(-R_{M4}\alpha_{1,ml}+R_{M3}\alpha_{2,ml})\beta_l^2-i\alpha_k(-R_{T4}\alpha_{1,ml}+R_{T3}\alpha_{2,ml})\alpha_m\beta_l\right]l_y=0
\end{aligned}\tag{76}$$

where

$$\alpha_m=k_x+\frac{2m\pi}{l_x},\quad \beta_n=k_y+\frac{2n\pi}{l_y}\tag{77}$$

Note that consideration of the virtual work in any other period of the structural element would have yielded an identical set of equations.

In order to separate the variants $\alpha_{1,kl}$ and $\alpha_{2,kl}$, Eqs. (75) and (76) are rewritten as

$$\begin{aligned}
&\left[D_1(\alpha_k^2+\beta_l^2)^2-m_1\omega^2-\frac{\omega^2\rho_0}{ik_{z,kl}}+\frac{\omega^2\rho_0\cos(k_{z,kl}d)}{k_{z,kl}\sin(k_{z,kl}d)}\right]l_xl_y\alpha_{1,kl}-\frac{\omega^2\rho_0}{k_{z,kl}\sin(k_{z,kl}d)}l_xl_y\alpha_{2,kl}\\
&\quad+\sum_{n=-\infty}^{+\infty}\left[R_{Q1}-i\alpha_k^3R_{M1}-i\beta_l\alpha_k\beta_nR_{T1}\right]l_x\alpha_{1,kn}+\sum_{n=-\infty}^{+\infty}\left[-R_{Q2}+i\alpha_k^3R_{M2}+i\beta_l\alpha_k\beta_nR_{T2}\right]l_x\alpha_{2,kn}\\
&\quad+\sum_{m=-\infty}^{+\infty}\left[R_{Q3}-i\beta_l^3R_{M3}-i\alpha_k\alpha_m\beta_lR_{T3}\right]l_y\alpha_{1,ml}+\sum_{m=-\infty}^{+\infty}\left[-R_{Q4}+i\beta_l^3R_{M4}+i\alpha_k\alpha_m\beta_lR_{T4}\right]l_y\alpha_{2,ml}\\
&=\begin{cases}2Il_xl_y & \text{when } k=0\&l=0\\ 0 & \text{when } k\neq0||l\neq0\end{cases}
\end{aligned}\tag{78}$$

$$\begin{aligned}
&\left[D_2(\alpha_k^2+\beta_l^2)^2-m_2\omega^2-\frac{\omega^2\rho_0}{ik_{z,kl}}+\frac{\omega^2\rho_0\cos(k_{z,kl}d)}{k_{z,kl}\sin(k_{z,kl}d)}\right]l_xl_y\alpha_{2,kl}-\frac{\omega^2\rho_0}{k_{z,kl}\sin(k_{z,kl}d)}l_xl_y\alpha_{1,kl}\\
&+\sum_{n=-\infty}^{+\infty}\left[-R_{Q2}+i\alpha_k^3R_{M2}+i\beta_l\alpha_k\beta_nR_{T2}\right]l_x\alpha_{1,kn}\quad+\sum_{n=-\infty}^{+\infty}\left[R_{Q1}-i\alpha_k^3R_{M1}-i\beta_l\alpha_k\beta_nR_{T1}\right]l_x\alpha_{2,kn}\\
&+\sum_{m=-\infty}^{+\infty}\left[-R_{Q4}+i\beta_l^3R_{M4}+i\alpha_k\alpha_m\beta_lR_{T4}\right]l_y\alpha_{1,ml}+\sum_{m=-\infty}^{+\infty}\left[R_{Q3}-i\beta_l^3R_{M3}-i\alpha_k\alpha_m\beta_lR_{T3}\right]l_y\alpha_{2,ml}=0
\end{aligned}\tag{79}$$

where the coupling relations between the modal amplitudes of sound waves in air and those of flexural waves in panels defined in Eqs. (57)–(61) have been included. Eqs. (78) and (79) form an infinite set of coupled algebraic simultaneous equations. The solution of a suitably restricted set of these equations allows the modal amplitudes $\alpha_{1,kl}$ and $\alpha_{2,kl}$ to be determined. Insofar as the solution converges, these equations are solved simultaneously by truncation, namely, restricting the sum-index (m, n) in the finite ranges of $m=-\hat{k}$ ***to*** $\hat{k}$ and $n=-\hat{l}$ ***to*** $\hat{l}$. With laborious but straightforward algebraic manipulations, the resulting simultaneous equations containing a finite number [i.e., $2KL$, where $K=2\hat{k}+1$, $L=2\hat{l}+1$] of unknowns can be grouped into matrix form, as

$$\begin{bmatrix}T_{11} & T_{12}\\ T_{21} & T_{22}\end{bmatrix}_{2KL\times2KL}\begin{Bmatrix}\alpha_{1,kl}\\ \alpha_{2,kl}\end{Bmatrix}_{2KL\times1}=\begin{Bmatrix}F_{kl}\\ 0\end{Bmatrix}_{2KL\times1}\tag{80}$$

Detailed derivations of Eq. (80) can be found in Appendix A. Once the unknowns $\alpha_{1,kl}$ and $\alpha_{2,kl}$ are determined by solving Eq. (80), the displacements (w_1, w_2) of the panels and the sound pressure (P_1, P_2, P_3) in the ambient acoustic fluids adjacent

to the two panels are also determined, enabling the sound transmission analysis of the fluid-loaded orthogonally rib-stiffened sandwich structure.

3. Definition of sound transmission loss

As can be seen from Eqs. (2) to (8), a component of the convective fluid-loaded pressure in the form of harmonic plane sound wave with wavenumbers (k_x, k_y) would induce sets of space harmonic wave components in the response (including sound pressure) with wavenumbers $(k_x+2m\pi/l_x, k_y+2n\pi/l_y)$, where (m, n) take values $(-\infty<m<+\infty, -\infty<n<+\infty)$. This implies that the groups of harmonic waves may travel in opposite directions. The appearance of the series of space harmonic waves in the response stems from the periodical rib-stiffeners attached to the panels. For a given convective fluid-loaded pressure with wavenumbers (k_x, k_y), a bending wave having the same wavenumbers is induced which then travels in the structure. The outspreading bending wave would be polarized as a group of harmonic wave components identified by wavenumbers $(a_0+2m\pi/l_x, \beta_0+2n\pi/l_y)$, owing to the complex interaction between the bending waves in panels and the motion of the mth x-wise and nth y-wise rib-stiffeners.

Given that (k_x, k_y) are real, the wavenumber $k_{z,mn}$ of the (m, n)th harmonic wave in the z-direction may be either real or pure imaginary (see Eqs. (10) and (11)). In the case of $k_{z,mn}$ being imaginary, the (m, n)th component of the wave decays exponentially with increasing distance in the z-direction and radiates no energy. This corresponds to a subsonic wave, i.e., non-radiating wave (Graham, 1995), satisfying that:

$$\left(k_x+\frac{2m\pi}{l_x}\right)^2+\left(k_y+\frac{2n\pi}{l_y}\right)^2>\left(\frac{\omega}{c_0}\right)^2 \tag{81}$$

Therefore, this (m, n)th component contributes only to the near field. Only when $k_{z,mn}$ is real, the (m, n)th component could contribute to the far field sound pressure (Mace, 1981; Xin et al., 2009b), which pertains to a supersonic wave, i.e., radiating wave (Graham, 1995), satisfying that:

$$\left(k_x+\frac{2m\pi}{l_x}\right)^2+\left(k_y+\frac{2n\pi}{l_y}\right)^2<\left(\frac{\omega}{c_0}\right)^2 \tag{82}$$

To facilitate the physical understanding of sound transmission, the transmission coefficient is defined here as the ratio of the transmitted sound power to the incident sound power, as

$$\tau(\varphi,\theta)=\frac{\sum_{m=-\infty}^{+\infty}\sum_{n=-\infty}^{+\infty}|\xi_{mn}|^2\,\mathrm{Re}(k_{z,mn})}{|I|^2 k_z} \tag{83}$$

which is dependent upon the incident angles ϕ and θ. Sound transmission loss (STL) is then customarily defined as the inverse of the power transmission coefficient in decibels scale (Xin and Lu, 2009; Xin et al., 2008b), as

$$STL=10\log_{10}\left(\frac{1}{\tau(\varphi,\theta)}\right) \tag{84}$$

Physically, STL is a measure of the effectiveness of the considered sandwich structure in isolating the transmission of convective fluid-loaded pressure.

4. Parametric investigation and discussions

Using the analytical model developed in the previous sections, we explore below the structural and acoustic behaviors of the infinite orthogonally rib-stiffened sandwich structure shown in Fig. 1 subjected to convective fluid-loaded pressure in terms of sound transmission loss characteristics.

For numerical analysis, it is assumed that the sandwich structure have two identical panels with thickness $h_1=h_2=0.002$ m, and orthogonal rib-stiffeners with depth $d=0.08$ m, identical thickness $t_x=t_y=0.001$ m, and identical periodicity spacing $l_x=l_y=0.2$ m (Fig. 1). The face panels and the rib-stiffeners are made of the same material, with Young's modulus $E=70$ GPa, density $\rho=2700$ kg/m^3, Poisson ratio $\nu=0.33$, and loss factor (introduced with the complex Young's modulus $\tilde{E}=E(1+i\eta)$) $\eta=0.01$. Air density is taken as $\rho_0=1.21$ kg/m^3 and sound speed in air as $c_0=343$ m/s. Since the viscosity of air is too small to exert a significant damping effect on the vibroacoustic response of the structure, it is not taken into account in the present analysis. Instead, the focus is placed on practically more important matters, such as the influence of inertial effects arising from rib-stiffener mass, the periodicity spacing of rib-stiffeners, and the airborne as well as structure-borne paths on sound transmission across the structure.

4.1. Convergence check for space-harmonic series solution

Since the analytical model is hinged on the assumed double-series solution given in Eqs. (2)–(8), a sufficiently large number of terms have to be used to ensure the convergence and accuracy of the solution. There exists an admissible criterion (Lee and Kim, 2002; Xin et al., 2010) that once the solution converges at a given frequency, it is also convergent

for all frequencies lower than that. Therefore, the needed number of series terms is determined by the highest frequency of interest (i.e., 10 kHz, the frequency range below which is of concern here). Convergence check is thus performed by calculating STL value at 10 kHz, with progressively more terms used in the double-series expansion (as shown in Fig. 3). Once the difference between two successive STL calculations falls within a pre-set error band (0.01 dB selected in this work), the solution is deemed to have converged and then the corresponding number of terms is adopted to calculate STL values at all other frequencies below 10 kHz.

In view of the symmetry of the present periodic structures in x- and y-direction, the equations are truncated as a finite set of equations with $m=-\hat{k}$ to $\hat{k}$ and $n=-\hat{l}$ to $\hat{l}$ ($\hat{k}=\hat{l}$ assumed) and then solved simultaneously. Fig. 3 shows the convergence tendency of STL solution as the single mode number $\hat{k}$ ($=\hat{l}$) is increased, when the sandwich structure is excited by a normally incident sound at 10 kHz. The results of Fig. 3 demonstrate that the solution converges when $\hat{k}\geq 19$. In other words, it needs at least 1521 terms (m and n both ranging from -19 to 19) to ensure solution convergence at 10 kHz. The same number (1521 terms) is employed in subsequent STL calculations below 10 kHz, sufficient for obtaining accurate results within the error bound of 0.01 dB.

4.2. Validation of the analytical model

The validity and feasibility of the proposed analytic model for sound transmission across an infinite orthogonally rib-stiffened sandwich structure subjected to convective fluid-loaded pressure is checked by comparing the model predictions and those obtained by Wang et al. (2005) for sound transmission through an infinite sandwich structure with parallel rib-stiffeners as the core. Whilst Wang et al. (2005) model a single rib-stiffener as a combination of translational spring and rotational spring, the tensional, bending and torsional vibrations of the rib-stiffener is modeled as an ensemble in the present analytic model. To make the comparison possible, the sets of orthogonal rib-stiffeners are simplified as one set of parallel rib-stiffeners. To this end, without loss of generality, the key parameters (i.e., Yong's modulus E_x, density ρ_x and thickness t_x) of the x-wise rib-stiffeners are set to zero, so that the orthogonally rib-stiffened sandwich construction is equivalent to an parallelly rib-stiffened sandwich structure. Of course, the material and geometrical properties of the structure adopted by Wang et al. (2005) are fully followed in the comparison.

To highlight the necessity and advantage of the exact consideration of rib-stiffener motions in sound transmission prediction for the whole structure, results obtained using both the complete model and the simplified model are compared with the predictions of Wang et al. (2005), as shown in Fig. 4. Here, the complete model proposed in Sections 2 and 3 not only treats the motions of the rib-stiffeners as an ensemble of tensional, bending and torsional vibrations, but also considers their inertial effects. The simplified model only retains the tensional forces, inertial tensional forces and bending moments of the y-wise rib-stiffeners in Eqs. (12) and (13), corresponding to the translational forces, inertial forces of lumped masses and rotational forces in Wang et al.'s model, respectively.

Overall, as illustrated in Fig. 4, the predictions of the simplified model agree well with those obtained by Wang et al. (2005). The visible discrepancies (at relatively high frequencies in particular) between the two models is attributable to the fact that, for simplicity, Wang et al. approximated the lumped mass per rib-stiffener as distributed mass which was then added to the panel mass. Whilst the STL versus frequency curves predicted by Wang et al. and the simplified model have an overall tendency of that predicted by the complete model, noticeable discrepancies are also observed in Fig. 4. This

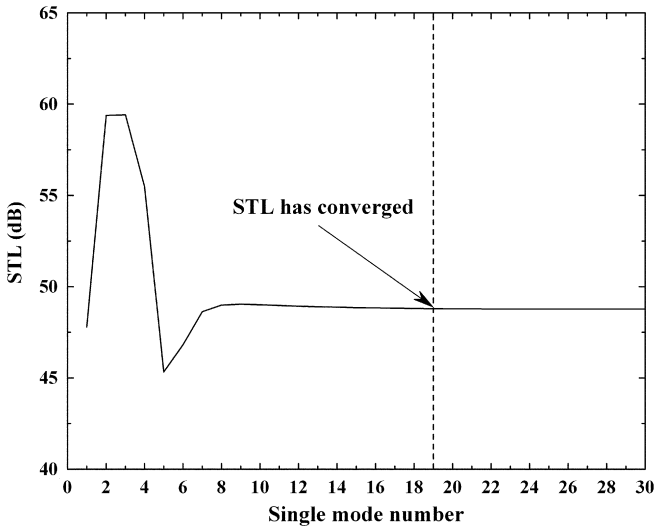

Fig. 3. Convergence check of double space-harmonic series solution for an infinite orthogonally rib-stiffened sandwich structure excited by a normally incident sound at 10 kHz.

confirms the necessity and advantage of the present analytical formulations for modeling the structural and acoustical behaviors of rib-stiffened sandwich structures subjected to convective fluid-loaded pressure.

4.3. *Influence of sound incident angles*

Since the incident azimuth angle θ plays a negligible role here, the influence of sound incident angle is mainly examined by comparing STL values calculated for three different incident elevation angles (i.e., φ=0°, 30°, 60°) with the azimuth angle fixed at θ=45°, as shown in Fig. 5.

The results of Fig. 5 demonstrate that the incident elevation angle has a significant effect on the STL of the present sandwich structure. It is observed that the first resonance dip is shifted to a lower frequency as the elevation angle is increased, and denser resonance dips appear on the STL versus frequency curves in the oblique incident case than those in the normal incident case. Accordingly, apart from several individual peaks, the averaged STL values are smaller than that in the normal incident case, particularly so in the low frequency range (below 400 Hz). In other words, the oblique incident

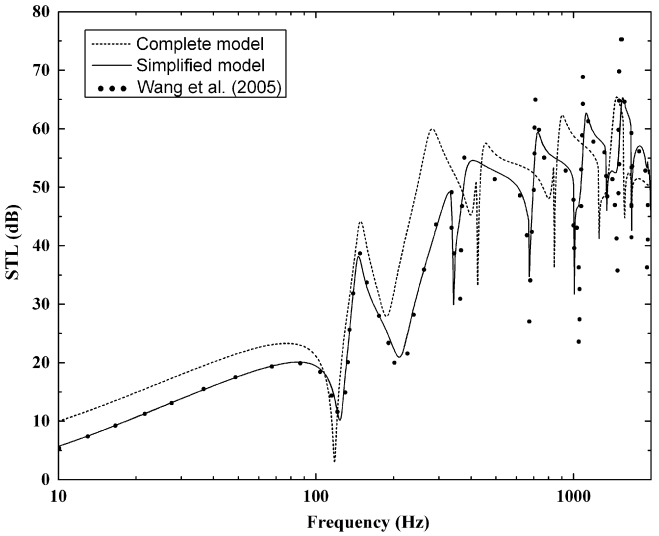

Fig. 4. Sound transmission loss plotted as a function of frequency for infinite sandwich structure with parallel rib-stiffeners as core subjected to oblique (φ=45°) incident sound: comparison between predictions by the present analytic model (both complete model and simplified model) and those by Wang et al. (2005).

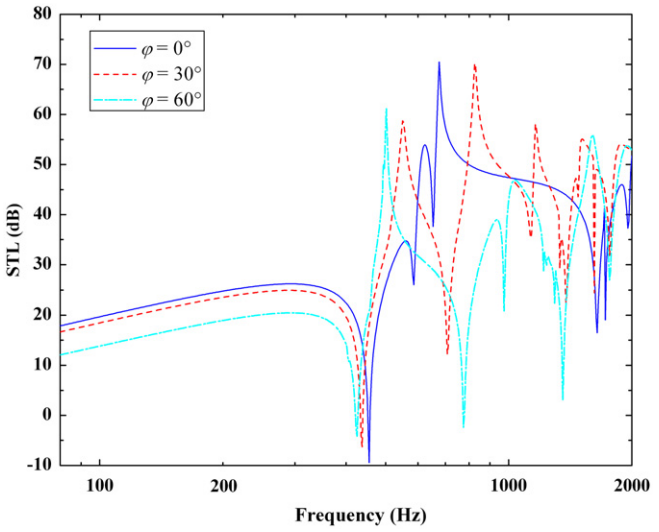

Fig. 5. Sound transmission loss plotted as a function of frequency for orthogonally rib-stiffened sandwich structure under sound excitation having selected incident angles.

sound power transmits through the structure more easily than that of the normal incident sound, due to the possibility of constructive interference between incident sound wave and structural bending waves in the former (Xin et al., 2009b).

Indeed, when the trace wavelength of incident sound matches the bending wave in the face panel of the sandwich, coincidence resonance occurs in the oblique incident case but not in the normal incident case (Fahy, 1985). Following Xin et al. (2009b), the coincidence resonance frequency may be analytically calculated as

$$f_c = \frac{c_0^2}{2\pi h \sin\varphi}\sqrt{\frac{12\rho(1-\nu^2)}{E}} \tag{85}$$

The coincident resonance appearing in the oblique case is often located at high frequencies that are beyond the frequency range considered in the present study. In view of the dense resonances of the sandwich structure itself and the complex interaction of bending waves in the face-panel and rib-stiffeners at high frequencies, the coincidence resonance dip would shift its original location and thus it is actually impossible to identify it especially in the present complex sandwich structures.

4.4. Influence of inertial effects arising from rib-stiffener mass

The inertial effects of rib-stiffener mass should not be ignored when the rib-stiffeners are heavy. To quantify the influence of inertial effects on sound transmission characteristics, Fig. 6 compares the predictions obtained for an orthogonally rib-stiffened sandwich structure with and without considering the inertial effects. The inertial effects of the rib-stiffeners on sound radiation from an orthogonally rib-stiffened sandwich subjected to harmonic point force excitation have been evaluated in a companion paper (Xin and Lu, submitted for publication). As such, the influence of inertial effects on sound transmission characteristics provides additional insight into the vibroacoustic dynamics of 2D periodic sandwich structures.

It is seen from Fig. 6 that the STL versus frequency curve predicted with the inertial effects considered has a tendency similar to that without considering the inertial effects, the main discrepancy being the existence of several additional peaks and dips in the former. On one hand, the superposition peaks (or dips) between the inertial case and the non-inertial one are dominated by face panel vibration, which are closely related to the maximum (or minimal) vibration patterns. On the other hand, the appearance of the additional peaks and dips controlled predominantly by the rib-stiffeners is attributed to the inertial effects arising from the mass of the rib-stiffeners.

4.5. Influence of rib-stiffener spacings

It is anticipated that the rib-stiffener spacings l_x and l_y (Fig. 1) characterizing the periodic nature of the 2D orthogonal sandwich play an important role in dictating the wave propagation and sound transmission performance of the structure. Their influence on the sound radiation behavior of the structure has been explored (Xin and Lu, submitted for publication), which are further examined below in terms of sound transmission.

Fig. 7 plots the STL as a function of frequency for two different orthogonally rib-stiffened sandwich structures, with (l_x, l_y) selected as (0.20, 0.20) and (0.25, 0.25) m, respectively. Within the low frequency range, it is seen from Fig. 7 that the

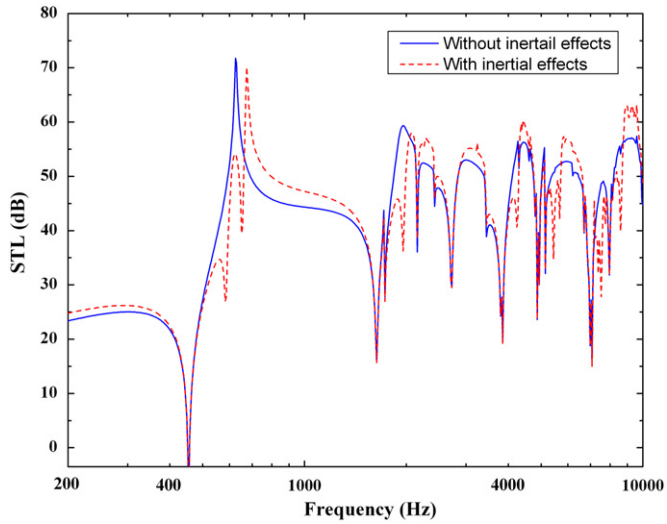

Fig. 6. Sound transmission loss plotted as a function of frequency for orthogonally rib-stiffened sandwich structure under normal incident sound: influence of inertial effects arising from rib-stiffener mass.

characteristic curves of sound transmission corresponding to two different periodicity spacings follow a similar trend, which is attributed to the fact that altering the periodicity spacings does not change the periodic nature of the sandwich markedly. However, at relatively high frequencies, visible discrepancies exist between the two cases. In addition, the STL peaks and dips are shifted to lower frequencies as the periodicity spacings increase, implying that the increment of periodicity spacings leads to noticeably reduced natural frequencies of the sandwich structure.

4.6. Influence of airborne and structure-borne paths

The incident sound can be transmitted via two routes from the upper panel to the bottom panel, namely, the structure-borne path (i.e., orthogonal rib-stiffeners) and the airborne path (i.e., air constrained in between the two panels). To illustrate the different roles played by the two different transmission paths, Fig. 8 compares the results obtained for three different cases: airborne path only (i.e., no rib-stiffeners), structure-borne path only (i.e., vacuum in cavity), and full sandwich structure.

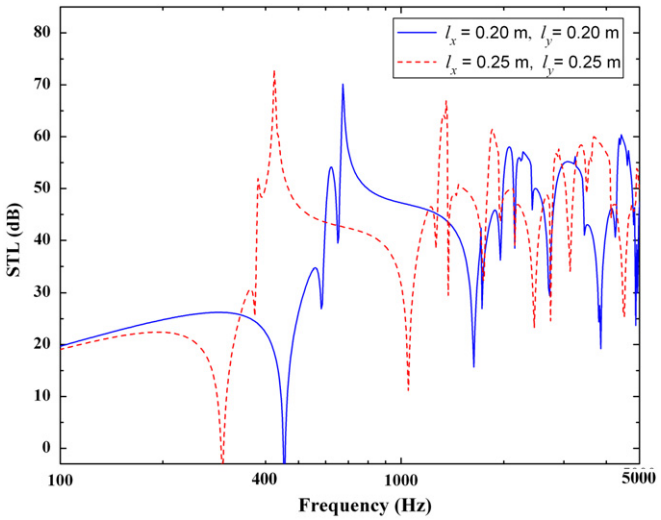

Fig. 7. Sound transmission loss plotted as a function of frequency for orthogonally rib-stiffened sandwich structure under normal incident sound: influence of periodicity spacings between rib-stiffeners.

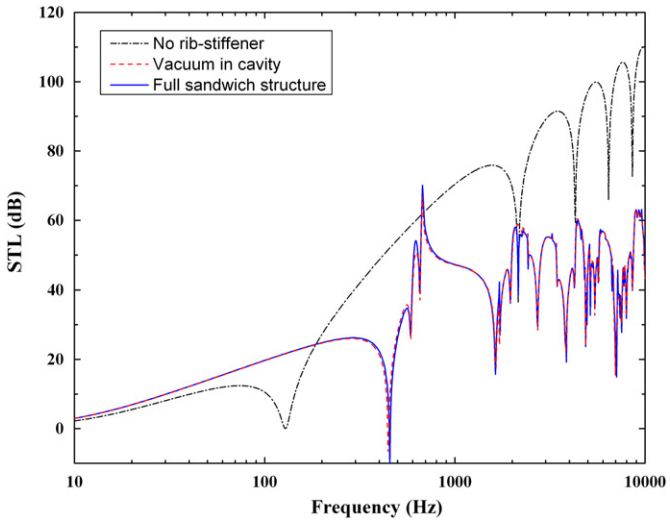

Fig. 8. Sound transmission loss plotted as a function of frequency for orthogonally rib-stiffened sandwich structure under normal incident sound: comparison between airborne and structure-borne transmission paths.

The results of Fig. 8 demonstrate that, insofar as sound transmission is of concern, the case of vacuum in cavity (structure-borne path only) is nearly identical to a full sandwich structure, both significantly different from the case of no rib-stiffeners. This is understandable, as the physical process of sound transmission across the sandwich is dominated by the structure-borne path, owing to the strong constraint of structural connections (rib-stiffeners) and weak fluid–structure coupling. However, it should be pointed out that, since the transmission of sound is of concern here, the fluid–structure coupling at the incident interface (i.e., between the incident side fluid and the upper panel) and the transmitting interface (i.e., between the transmitting side fluid and the bottom panel) needs to be considered. Although the fluid–structure coupling between the air cavity and the internal interfaces of the two panels is negligibly weak compared to the constraint imposed by the rib-stiffeners, for preciseness in physics and mathematics, this coupling is included in the present analysis (which does not need much additional efforts).

In the absence of the rib-stiffeners, the first dip of the STL curve in Fig. 8 corresponds to the 'mass–air–mass' resonance $f_a=\sqrt{\rho_0 c_0^2(m_1+m_2)/(m_1 m_2 d)}/2\pi$, whilst the following four dips (and those not shown in Fig. 8) are related to the standing wave resonance $f_{s,n}=nc_0/2d$, where $n=1, 2, 3, 4\ldots$ (Lin and Garrelick, 1977; Xin and Lu, 2009; Xin et al., 2008b, 2009a, b). In the case of full sandwich structure, the complex interaction of flexural wave in the panel and the rib-stiffeners creates multiple possibilities for wavenumber matching and 'coincidence' (Wang et al., 2005), causing a series of resonance dips appearing in the STL curve that differ significantly from the no rib-stiffener case.

5. Conclusions

Rigorous analytical formulations are obtained with the space harmonic approach for the structural and acoustical characteristics of an infinite orthogonally rib-stiffened sandwich structure subjected to convective fluid-loaded pressure. Unlike previous studies that focus on relatively simple structures such as rib-stiffened plates and model approximately the rib-stiffeners as Euler-beams, two-dimensionally periodic sandwiches stiffened by two sets of orthogonally rib-stiffeners are considered. All possible motions of the rib-stiffeners are accurately accounted for by introducing their tensional forces, bending moments and torsional moments as well as the corresponding inertial terms into the governing equations of the two face panels. The surrounding acoustic fluids are restricted by the acoustic wave equation and fluid–structure coupling is included by imposing velocity continuity conditions at fluid–panel interfaces. Built upon the Bloch/Floquet theorem for periodic structures, the resulting panel motions and acoustic pressures are expressed in a superposition form of space harmonics for a given wavenumber. The application of the virtual work principle for one periodic element yields two infinite sets of simultaneous algebraic coupled equations, which are numerically solved by truncation.

To explore the physical mechanisms underlying the dynamic and acoustic performance of two-dimensionally periodic sandwich structures, the analysis is carried out from the viewpoint of sound transmission. Firstly, the validity and feasibility of the proposed analytic model is qualified by comparing the model predictions with previous published results for one-dimensionally periodic sandwich structures. The necessity and advantage of the exact modeling of rib-stiffener vibrations are also demonstrated by comparing the complete model, with its simplified version and the model of Wang et al. (2005). The complete model is then used to quantify the influences of inertial effects arising from the rib-stiffener mass, the airborne and structure-borne paths, and the periodicity spacings of the rib-stiffeners on sound transmission across the sandwich structure.

Although the analytical model without considering the inertial effects of the rib-stiffeners is able to provide an overall trend of the STL versus frequency curve, the inclusion of the inertial effects in the model enables the capturing of more detailed physical features associated with the process of sound transmission, as reflected by the additional peaks and dips appearing on the STL curve.

The periodicity spacings of the rib-stiffeners play an important role in transmitting the sound across the sandwich. Two noticeable conclusions can be drawn. First, as slight alterations of the periodicity spacings do not change the periodical nature of the structure, the STL curves of different spacings exhibit similar trends. Second, increasing the periodicity spacings reduces the natural frequencies of the structure, reflected by the shifting of STL peaks and dips to lower frequencies.

For sandwich structure reinforced with rib-stiffeners, the transmission of sound via the airborne route is negligible in comparison with that transmitted via the structure-borne path, as the weak fluid–structure coupling is overwhelmed by the strong structural connections (rib-stiffeners). However, for preciseness in the viewpoints of physics and mathematics, the fluid–structure coupling present between the incident side fluid and the upper panel as well as that between the transmitting side fluid and the bottom panel needs to be considered in the analysis of sound transmission.

Acknowledgements

This work is supported by the National Basic Research Program of China (2006CB601202), the National 111 Project of China (B06024) and the National Natural Science Foundation of China (10825210).

Appendix A. Derivation of Eq. (80)

The deflection coefficients of the two face panels are:

$$\{\alpha_{1,kl}\}=\left[\begin{array}{cccccccccc}\alpha_{1,11} & \alpha_{1,21} & \dots & \alpha_{1,K1} & \alpha_{1,12} & \alpha_{1,22} & \dots & \alpha_{1,K2} & \dots & \alpha_{1,KL}\end{array}\right]^{\mathbf{T}}_{KL\times 1} \tag{A.1}$$

$$\{\alpha_{2,kl}\}=\left[\begin{array}{cccccccccc}\alpha_{2,11} & \alpha_{2,21} & \dots & \alpha_{2,K1} & \alpha_{2,12} & \alpha_{2,22} & \dots & \alpha_{2,K2} & \dots & \alpha_{2,KL}\end{array}\right]^{\mathbf{T}}_{KL\times 1} \tag{A.2}$$

The right-hand side of Eq. (80) represents the generalized force, that is:

$$\{F_{kl}\}=\left[\begin{array}{cccccccccc}F_{11} & F_{21} & \dots & F_{K1} & F_{12} & F_{22} & \dots & F_{K2} & \dots & F_{KL}\end{array}\right]^{\mathbf{T}}_{KL\times 1} \tag{A.3}$$

where

$$F_{kl}=\begin{cases}2Il_xl_y & \text{at } k=\dfrac{K+1}{2} \text{ and } l=\dfrac{L+1}{2}\\ 0 & \text{at } k\neq\dfrac{K+1}{2}\parallel l\neq\dfrac{L+1}{2}\end{cases} \tag{A.4}$$

$$\lambda_{kl}^{11,1}=\left[D_1(\alpha_k^2+\beta_l^2)^2-m_1\omega^2-\frac{\omega^2\rho_0}{ik_{z,kl}}+\frac{\omega^2\rho_0\cos(k_{z,kl}d)}{k_{z,kl}\sin(k_{z,kl}d)}\right]l_xl_y \tag{A.5}$$

$$T_{11,1}=\left[\begin{array}{ccccccccccc}\lambda_{11}^{11,1} & & & & & & & & & & \\ & \lambda_{21}^{11,1} & & & & & & & & & \\ & & \ddots & & & & & & & & \\ & & & \lambda_{K1}^{11,1} & & & & & & & \\ & & & & \lambda_{12}^{11,1} & & & & & & \\ & & & & & \lambda_{22}^{11,1} & & & & & \\ & & & & & & \ddots & & & & \\ & & & & & & & \lambda_{K2}^{11,1} & & & \\ & & & & & & & & \ddots & & \\ & & & & & & & & & \lambda_{KL}^{11,1} & \end{array}\right]_{KL\times KL} \tag{A.6}$$

$$\lambda_{KL}^{11,2}=l_x\left[\begin{array}{ccccc}R_{Q1}-i\alpha_1^3R_{M1} & & & & \\ & R_{Q1}-i\alpha_2^3R_{M1} & & & \\ & & \ddots & & \\ & & & R_{Q1}-i\alpha_K^3R_{M1} & \end{array}\right]_{K\times L} \tag{A.7}$$

$$T_{11,2}=\left[\begin{array}{cccc}\lambda_{KL}^{11,2} & \lambda_{KL}^{11,2} & \dots & \lambda_{KL}^{11,2}\\ \lambda_{KL}^{11,2} & \lambda_{KL}^{11,2} & \dots & \lambda_{KL}^{11,2}\\ \vdots & \vdots & \ddots & \vdots\\ \lambda_{KL}^{11,2} & \lambda_{KL}^{11,2} & \dots & \lambda_{KL}^{11,2}\end{array}\right]_{KL\times KL} \tag{A.8}$$

$$\lambda_{Kl,n}^{11,3}=l_x\left[\begin{array}{ccccc}-i\alpha_1\beta_l\beta_nR_{T1} & & & & \\ & -i\alpha_2\beta_l\beta_nR_{T1} & & & \\ & & \ddots & & \\ & & & -i\alpha_K\beta_l\beta_nR_{T1} & \end{array}\right]_{K\times L} \tag{A.9}$$

$$T_{11,3}=\left[\begin{array}{cccc}\lambda_{K1,1}^{11,3} & \lambda_{K1,2}^{11,3} & \dots & \lambda_{K1,L}^{11,3}\\ \lambda_{K2,1}^{11,3} & \lambda_{K2,2}^{11,3} & \dots & \lambda_{K2,L}^{11,3}\\ \vdots & \vdots & \ddots & \vdots\\ \lambda_{KL,1}^{11,3} & \lambda_{KL,2}^{11,3} & \dots & \lambda_{KL,L}^{11,3}\end{array}\right]_{KL\times KL} \tag{A.10}$$

$$\lambda_{Kl}^{11,4}=l_y\begin{bmatrix} R_{Q3}-i\beta_l^3R_{M3} & R_{Q3}-i\beta_l^3R_{M3} & \dots & R_{Q3}-i\beta_l^3R_{M3}\\ R_{Q3}-i\beta_l^3R_{M3} & R_{Q3}-i\beta_l^3R_{M3} & \dots & R_{Q3}-i\beta_l^3R_{M3}\\ \vdots & \vdots & \ddots & \vdots\\ R_{Q3}-i\beta_l^3R_{M3} & R_{Q3}-i\beta_l^3R_{M3} & \dots & R_{Q3}-i\beta_l^3R_{M3}\end{bmatrix}_{K\times L} \tag{A.11}$$

$$T_{11,4}=\begin{bmatrix}\lambda_{K1}^{11,4} & & & \\ & \lambda_{K2}^{11,4} & & \\ & & \ddots & \\ & & & \lambda_{KL}^{11,4}\end{bmatrix}_{KL\times KL} \tag{A.12}$$

$$\lambda_{Kl}^{11,5}=l_y\begin{bmatrix} -i\alpha_1\beta_l\alpha_1R_{T3} & -i\alpha_1\beta_l\alpha_2R_{T3} & \dots & -i\alpha_1\beta_l\alpha_KR_{T3}\\ -i\alpha_2\beta_l\alpha_1R_{T3} & -i\alpha_2\beta_l\alpha_2R_{T3} & \dots & -i\alpha_2\beta_l\alpha_KR_{T3}\\ \vdots & \vdots & \ddots & \vdots\\ -i\alpha_K\beta_l\alpha_1R_{T3} & -i\alpha_K\beta_l\alpha_2R_{T3} & \dots & -i\alpha_K\beta_l\alpha_KR_{T3}\end{bmatrix}_{K\times L} \tag{A.13}$$

$$T_{11,5}=\begin{bmatrix}\lambda_{K1}^{11,5} & & & \\ & \lambda_{K2}^{11,5} & & \\ & & \ddots & \\ & & & \lambda_{KL}^{11,5}\end{bmatrix}_{KL\times KL} \tag{A.14}$$

$$\lambda_{kl}^{12,1}=-\frac{\omega^2\rho_0}{k_{z,kl}\sin(k_{z,kl}d)}l_xl_y \tag{A.15}$$

$$T_{12,1}=\begin{bmatrix}\lambda_{11}^{12,1} & & & & & & & & & \\ & \lambda_{21}^{12,1} & & & & & & & & \\ & & \ddots & & & & & & & \\ & & & \lambda_{K1}^{12,1} & & & & & & \\ & & & & \lambda_{12}^{12,1} & & & & & \\ & & & & & \lambda_{22}^{12,1} & & & & \\ & & & & & & \ddots & & & \\ & & & & & & & \lambda_{K2}^{12,1} & & \\ & & & & & & & & \ddots & \\ & & & & & & & & & \lambda_{KL}^{12,1}\end{bmatrix}_{KL\times KL} \tag{A.16}$$

$$\lambda_{KL}^{12,2}=l_x\begin{bmatrix}-R_{Q2}+i\alpha_1^3R_{M2} & & & \\ & -R_{Q2}+i\alpha_2^3R_{M2} & & \\ & & \ddots & \\ & & & -R_{Q2}+i\alpha_K^3R_{M2}\end{bmatrix}_{K\times L} \tag{A.17}$$

$$T_{12,2}=\begin{bmatrix}\lambda_{KL}^{12,2} & \lambda_{KL}^{12,2} & \dots & \lambda_{KL}^{12,2}\\ \lambda_{KL}^{12,2} & \lambda_{KL}^{12,2} & \dots & \lambda_{KL}^{12,2}\\ \vdots & \vdots & \ddots & \vdots\\ \lambda_{KL}^{12,2} & \lambda_{KL}^{12,2} & \dots & \lambda_{KL}^{12,2}\end{bmatrix}_{KL\times KL} \tag{A.18}$$

$$\lambda_{Kl,n}^{12,3}=l_x\begin{bmatrix}i\alpha_1\beta_l\beta_nR_{T2} & & & \\ & i\alpha_2\beta_l\beta_nR_{T2} & & \\ & & \ddots & \\ & & & i\alpha_K\beta_l\beta_nR_{T2}\end{bmatrix}_{K\times L} \tag{A.19}$$

$$T_{12,3}=\begin{bmatrix}\lambda_{K1,1}^{12,3} & \lambda_{K1,2}^{12,3} & \cdots & \lambda_{K1,L}^{12,3}\\ \lambda_{K2,1}^{12,3} & \lambda_{K2,2}^{12,3} & \cdots & \lambda_{K2,L}^{12,3}\\ \vdots & \vdots & \ddots & \vdots\\ \lambda_{KL,1}^{12,3} & \lambda_{KL,2}^{12,3} & \cdots & \lambda_{KL,L}^{12,3}\end{bmatrix}_{KL\times KL} \tag{A.20}$$

$$\lambda_{Kl}^{12,4}=l_y\begin{bmatrix}-R_{Q4}+i\beta_l^3R_{M4} & -R_{Q4}+i\beta_l^3R_{M4} & \cdots & -R_{Q4}+i\beta_l^3R_{M4}\\ -R_{Q4}+i\beta_l^3R_{M4} & -R_{Q4}+i\beta_l^3R_{M4} & \cdots & -R_{Q4}+i\beta_l^3R_{M4}\\ \vdots & \vdots & \ddots & \vdots\\ -R_{Q4}+i\beta_l^3R_{M4} & -R_{Q4}+i\beta_l^3R_{M4} & \cdots & -R_{Q4}+i\beta_l^3R_{M4}\end{bmatrix}_{K\times L} \tag{A.21}$$

$$T_{12,4}=\begin{bmatrix}\lambda_{K1}^{12,4} & & & \\ & \lambda_{K2}^{12,4} & & \\ & & \ddots & \\ & & & \lambda_{KL}^{12,4}\end{bmatrix}_{KL\times KL} \tag{A.22}$$

$$\lambda_{Kl}^{12,5}=l_y\begin{bmatrix}i\alpha_1\beta_l\alpha_1R_{T4} & i\alpha_1\beta_l\alpha_2R_{T4} & \cdots & i\alpha_1\beta_l\alpha_KR_{T4}\\ i\alpha_2\beta_l\alpha_1R_{T4} & i\alpha_2\beta_l\alpha_2R_{T4} & \cdots & i\alpha_2\beta_l\alpha_KR_{T4}\\ \vdots & \vdots & \ddots & \vdots\\ i\alpha_K\beta_l\alpha_1R_{T4} & i\alpha_K\beta_l\alpha_2R_{T4} & \cdots & i\alpha_K\beta_l\alpha_KR_{T4}\end{bmatrix}_{K\times L} \tag{A.23}$$

$$T_{12,5}=\begin{bmatrix}\lambda_{K1}^{12,5} & & & \\ & \lambda_{K2}^{12,5} & & \\ & & \ddots & \\ & & & \lambda_{KL}^{12,5}\end{bmatrix}_{KL\times KL} \tag{A.24}$$

$$\lambda_{kl}^{21,1}=-\frac{\omega^2\rho_0}{k_{z,kl}\sin(k_{z,kl}d)}l_xl_y \tag{A.25}$$

$$T_{21,1}=\begin{bmatrix}\lambda_{11}^{21,1} & & & & & & & & & \\ & \lambda_{21}^{21,1} & & & & & & & & \\ & & \ddots & & & & & & & \\ & & & \lambda_{K1}^{21,1} & & & & & & \\ & & & & \lambda_{12}^{21,1} & & & & & \\ & & & & & \lambda_{22}^{21,1} & & & & \\ & & & & & & \ddots & & & \\ & & & & & & & \lambda_{K2}^{21,1} & & \\ & & & & & & & & \ddots & \\ & & & & & & & & & \lambda_{KL}^{21,1}\end{bmatrix}_{KL\times KL} \tag{A.26}$$

$$\lambda_{KL}^{21,2}=l_x\begin{bmatrix}-R_{Q2}+i\alpha_1^3R_{M2} & & & \\ & -R_{Q2}+i\alpha_2^3R_{M2} & & \\ & & \ddots & \\ & & & -R_{Q2}+i\alpha_K^3R_{M2}\end{bmatrix}_{K\times L} \tag{A.27}$$

$$T_{21,2}=\begin{bmatrix}\lambda_{KL}^{21,2} & \lambda_{KL}^{21,2} & \cdots & \lambda_{KL}^{21,2}\\ \lambda_{KL}^{21,2} & \lambda_{KL}^{21,2} & \cdots & \lambda_{KL}^{21,2}\\ \vdots & \vdots & \ddots & \vdots\\ \lambda_{KL}^{21,2} & \lambda_{KL}^{21,2} & \cdots & \lambda_{KL}^{21,2}\end{bmatrix}_{KL\times KL} \tag{A.28}$$

$$\lambda_{Kl,n}^{21,3}=l_x\begin{bmatrix} i\alpha_1\beta_l\beta_n R_{T2} & & & \\ & i\alpha_2\beta_l\beta_n R_{T2} & & \\ & & \ddots & \\ & & & i\alpha_K\beta_l\beta_n R_{T2}\end{bmatrix}_{K\times L} \tag{A.29}$$

$$T_{21,3}=\begin{bmatrix} \lambda_{K1,1}^{21,3} & \lambda_{K1,2}^{21,3} & \cdots & \lambda_{K1,L}^{21,3} \\ \lambda_{K2,1}^{21,3} & \lambda_{K2,2}^{21,3} & \cdots & \lambda_{K2,L}^{21,3} \\ \vdots & \vdots & \ddots & \vdots \\ \lambda_{KL,1}^{21,3} & \lambda_{KL,2}^{21,3} & \cdots & \lambda_{KL,L}^{21,3}\end{bmatrix}_{KL\times KL} \tag{A.30}$$

$$\lambda_{Kl}^{21,4}=l_y\begin{bmatrix} -R_{Q4}+i\beta_l^3R_{M4} & -R_{Q4}+i\beta_l^3R_{M4} & \cdots & -R_{Q4}+i\beta_l^3R_{M4} \\ -R_{Q4}+i\beta_l^3R_{M4} & -R_{Q4}+i\beta_l^3R_{M4} & \cdots & -R_{Q4}+i\beta_l^3R_{M4} \\ \vdots & \vdots & \ddots & \vdots \\ -R_{Q4}+i\beta_l^3R_{M4} & -R_{Q4}+i\beta_l^3R_{M4} & \cdots & -R_{Q4}+i\beta_l^3R_{M4}\end{bmatrix}_{K\times L} \tag{A.31}$$

$$T_{21,4}=\begin{bmatrix} \lambda_{K1}^{21,4} & & & \\ & \lambda_{K2}^{21,4} & & \\ & & \ddots & \\ & & & \lambda_{KL}^{21,4}\end{bmatrix}_{KL\times KL} \tag{A.32}$$

$$\lambda_{Kl}^{21,5}=l_y\begin{bmatrix} i\alpha_1\beta_l\alpha_1R_{T4} & i\alpha_1\beta_l\alpha_2R_{T4} & \cdots & i\alpha_1\beta_l\alpha_KR_{T4} \\ i\alpha_2\beta_l\alpha_1R_{T4} & i\alpha_2\beta_l\alpha_2R_{T4} & \cdots & i\alpha_2\beta_l\alpha_KR_{T4} \\ \vdots & \vdots & \ddots & \vdots \\ i\alpha_K\beta_l\alpha_1R_{T4} & i\alpha_K\beta_l\alpha_2R_{T4} & \cdots & i\alpha_K\beta_l\alpha_KR_{T4}\end{bmatrix}_{K\times L} \tag{A.33}$$

$$T_{21,5}=\begin{bmatrix} \lambda_{K1}^{21,5} & & & \\ & \lambda_{K2}^{21,5} & & \\ & & \ddots & \\ & & & \lambda_{KL}^{21,5}\end{bmatrix}_{KL\times KL} \tag{A.34}$$

$$\lambda_{kl}^{22,1}=\left[D_2(\alpha_k^2+\beta_l^2)^2-m_2\omega^2-\frac{\omega^2\rho_0}{ik_{z,kl}}+\frac{\omega^2\rho_0\cos(k_{z,kl}d)}{k_{z,kl}\sin(k_{z,kl}d)}\right]l_xl_y \tag{A.35}$$

$$T_{22,1}=\begin{bmatrix} \lambda_{11}^{22,1} & & & & & & & & & \\ & \lambda_{21}^{22,1} & & & & & & & & \\ & & \ddots & & & & & & & \\ & & & \lambda_{K1}^{22,1} & & & & & & \\ & & & & \lambda_{12}^{22,1} & & & & & \\ & & & & & \lambda_{22}^{22,1} & & & & \\ & & & & & & \ddots & & & \\ & & & & & & & \lambda_{K2}^{22,1} & & \\ & & & & & & & & \ddots & \\ & & & & & & & & & \lambda_{KL}^{22,1}\end{bmatrix}_{KL\times KL} \tag{A.36}$$

$$\lambda_{KL}^{22,2}=l_x\begin{bmatrix} R_{Q1}-i\alpha_1^3R_{M1} & & & \\ & R_{Q1}-i\alpha_2^3R_{M1} & & \\ & & \ddots & \\ & & & R_{Q1}-i\alpha_K^3R_{M1}\end{bmatrix}_{K\times L} \tag{A.37}$$

$$T_{22,2}=\begin{bmatrix}\lambda_{KL}^{22,2} & \lambda_{KL}^{22,2} & \cdots & \lambda_{KL}^{22,2}\\ \lambda_{KL}^{22,2} & \lambda_{KL}^{22,2} & \cdots & \lambda_{KL}^{22,2}\\ \vdots & \vdots & \ddots & \vdots\\ \lambda_{KL}^{22,2} & \lambda_{KL}^{22,2} & \cdots & \lambda_{KL}^{22,2}\end{bmatrix}_{KL\times KL} \tag{A.38}$$

$$\lambda_{Kl,n}^{22,3}=l_x\begin{bmatrix}-i\alpha_1\beta_l\beta_n R_{T1} & & & \\ & -i\alpha_2\beta_l\beta_n R_{T1} & & \\ & & \ddots & \\ & & & -i\alpha_K\beta_l\beta_n R_{T1}\end{bmatrix}_{K\times L} \tag{A.39}$$

$$T_{22,3}=\begin{bmatrix}\lambda_{K1,1}^{22,3} & \lambda_{K1,2}^{22,3} & \cdots & \lambda_{K1,L}^{22,3}\\ \lambda_{K2,1}^{22,3} & \lambda_{K2,2}^{22,3} & \cdots & \lambda_{K2,L}^{22,3}\\ \vdots & \vdots & \ddots & \vdots\\ \lambda_{KL,1}^{22,3} & \lambda_{KL,2}^{22,3} & \cdots & \lambda_{KL,L}^{22,3}\end{bmatrix}_{KL\times KL} \tag{A.40}$$

$$\lambda_{Kl}^{22,4}=l_y\begin{bmatrix}R_{Q3}-i\beta_l^3R_{M3} & R_{Q3}-i\beta_l^3R_{M3} & \cdots & R_{Q3}-i\beta_l^3R_{M3}\\ R_{Q3}-i\beta_l^3R_{M3} & R_{Q3}-i\beta_l^3R_{M3} & \cdots & R_{Q3}-i\beta_l^3R_{M3}\\ \vdots & \vdots & \ddots & \vdots\\ R_{Q3}-i\beta_l^3R_{M3} & R_{Q3}-i\beta_l^3R_{M3} & \cdots & R_{Q3}-i\beta_l^3R_{M3}\end{bmatrix}_{K\times L} \tag{A.41}$$

$$T_{22,4}=\begin{bmatrix}\lambda_{K1}^{22,4} & & & \\ & \lambda_{K2}^{22,4} & & \\ & & \ddots & \\ & & & \lambda_{KL}^{22,4}\end{bmatrix}_{KL\times KL} \tag{A.42}$$

$$\lambda_{Kl}^{22,5}=l_y\begin{bmatrix}-i\alpha_1\beta_l\alpha_1R_{T3} & -i\alpha_1\beta_l\alpha_2R_{T3} & \cdots & -i\alpha_1\beta_l\alpha_KR_{T3}\\ -i\alpha_2\beta_l\alpha_1R_{T3} & -i\alpha_2\beta_l\alpha_2R_{T3} & \cdots & -i\alpha_2\beta_l\alpha_KR_{T3}\\ \vdots & \vdots & \ddots & \vdots\\ -i\alpha_K\beta_l\alpha_1R_{T3} & -i\alpha_K\beta_l\alpha_2R_{T3} & \cdots & -i\alpha_K\beta_l\alpha_KR_{T3}\end{bmatrix}_{K\times L} \tag{A.43}$$

$$T_{22,5}=\begin{bmatrix}\lambda_{K1}^{22,5} & & & \\ & \lambda_{K2}^{22,5} & & \\ & & \ddots & \\ & & & \lambda_{KL}^{22,5}\end{bmatrix}_{KL\times KL} \tag{A.44}$$

Using the definition of the sub-matrices presented above, one obtains

$$T_{11}=T_{11,1}+T_{11,2}+T_{11,3}+T_{11,4}+T_{11,5},\quad T_{22}=T_{22,1}+T_{22,2}+T_{22,3}+T_{22,4}+T_{22,5} \tag{A.45}$$

$$T_{12}=T_{12,1}+T_{12,2}+T_{12,3}+T_{12,4}+T_{12,5},\quad T_{21}=T_{21,1}+T_{21,2}+T_{21,3}+T_{21,4}+T_{21,5} \tag{A.46}$$

References

Brillouin, L., 1953. In: Wave Propagation in Periodic Structures. Dover, New York.

Cooper, A.J., Crighton, D.G., 1998a. Transmission of energy down periodically ribbed elastic structures under fluid loading: algebraic decay in the stop bands. Proc. R. Soc. London A 454, 1337–1355.

Cooper, A.J., Crighton, D.G., 1998b. Transmission of energy down periodically ribbed elastic structures under fluid loading: spatial periodicity in the pass bands. Proc. R. Soc. London A 454, 2893–2909.

Crighton, D.G., 1984. Transmission of energy down periodically ribbed elastic structures under fluid loading. Proc. R. Soc. London A 394, 405–436.

Dozio, L., Ricciardi, M., 2009. Free vibration analysis of ribbed plates by a combined analytical–numerical method. J. Sound Vib. 319, 681–697.

Fahy, F., 1985. In: Sound and Structural Vibration: Radiation, Transmission and Response. Academic Press, London.

Fahy, F.J., Lindqvist, E., 1976. Wave propagation in damped, stiffened structures characteristic of ship construction. J. Sound Vib. 45, 115–138.

Graham, W.R., 1995. High-frequency vibration and acoustic radiation of fluid-loaded plates. Proc. R. Soc. London A 352, 1–43.

Hambric, S.A., Hwang, Y.F., Bonness, W.K., 2004. Vibrations of plates with clamped and free edges excited by low-speed turbulent boundary layer flow. J. Fluid Struct. 19, 93–110.

Ichchou, M.N., Berthaut, J., Collet, M., 2008a. Multi-mode wave propagation in ribbed plates. Part I: wavenumber-space characteristics. Int. J. Solids Struct. 45, 1179–1195.

Ichchou, M.N., Berthaut, J., Collet, M., 2008b. Multi-mode wave propagation in ribbed plates. Part ii: predictions and comparisons. Int. J. Solids Struct. 45, 1196–1216.

Langley, R.S., Bardell, N.S., Ruivo, H.M., 1997. The response of two-dimensional periodic structures to harmonic point loading: a theoretical and experimental study of a beam grillage. J. Sound Vib. 207, 521–535.
Lee, J.H., Kim, J., 2002. Analysis of sound transmission through periodically stiffened panels by space-harmonic expansion method. J. Sound Vib. 251, 349–366.
Legault, J., Atalla, N., 2009. Numerical and experimental investigation of the effect of structural links on the sound transmission of a lightweight double panel structure. J. Sound Vib. 324, 712–732.
Leppington, F.G., 1989. The transmission of randomly incident sound through an elastic panel. Proc. R. Soc. London A 426, 153–165.
Leppington, F.G., Broadbent, E.G., Heron, K.H., 1984. Acoustic radiation from rectangular panels with constrained edges. Proc. R. Soc. London A 393, 67–84.
Leppington, F.G., Broadbent, E.G., Heron, K.H., Mead, S.M., 1986. Resonant and non-resonant acoustic properties of elastic panels. I. The radiation problem. Proc. R. Soc. London A 406, 139–171.
Leppington, F.G., Heron, K.H., Broadbent, E.G., 2002. Resonant and non-resonant transmission of random noise through complex plates. Proc. R. Soc. London A 458, 683–704.
Leppington, F.G., Heron, K.H., Broadbent, E.G., Mead, S.M., 1987. Resonant and non-resonant acoustic properties of elastic panels. Ii. The transmission problem. Proc. R. Soc. London A 412, 309–337.
Li, F.-M., Wang, Y.-S., 2005. Study on wave localization in disordered periodic layered piezoelectric composite structures. Int. J. Solids Struct. 42, 6457–6474.
Li, F.M., Wang, Y.S., Hu, C., Huang, W.H., 2005. Localization of elastic waves in periodic rib-stiffened rectangular plates under axial compressive load. J. Sound Vib. 281, 261–273.
Lin, G.-F., Garrelick, J.M., 1977. Sound transmission through periodically framed parallel plates. J. Acoust. Soc. Am. 61, 1014–1018.
Liu, L., Bhattacharya, K., 2009. Wave propagation in a sandwich structure. Int. J. Solids Struct. 46, 3290–3300.
Lucey, A.D., 1998. The excitation of waves on a flexible panel in a uniform flow. Proc. R. Soc. London A 356, 2999–3039.
Mace, B.R., 1980a. Periodically stiffened fluid-loaded plates, i: response to convected harmonic pressure and free wave propagation. J. Sound Vib. 73, 473–486.
Mace, B.R., 1980b. Periodically stiffened fluid-loaded plates, ii: response to line and point forces. J. Sound Vib. 73, 487–504.
Mace, B.R., 1980c. Sound radiation from a plate reinforced by two sets of parallel stiffeners. J. Sound Vib. 71, 435–441.
Mace, B.R., 1981. Sound radiation from fluid loaded orthogonally stiffened plates. J. Sound Vib. 79, 439–452.
Mace, B.R., 1996. The vibration of plates on two-dimensionally periodic point supports. J. Sound Vib. 192, 629–643.
Maury, C., Gardonio, P., Elliott, S.J., 2001. Active control of the flow-induced noise transmitted through a panel. AIAA J. 39, 1860–1867.
Maxit, L., 2009. Wavenumber space and physical space responses of a periodically ribbed plate to a point drive: a discrete approach. Appl. Acoust. 70, 563–578.
Mead, D.J., 1970. Free wave propagation in periodically supported, infinite beams. J. Sound Vib. 11, 181–197.
Mead, D.J., 1996. Wave propagation in continuous periodic structures: research contributions from Southampton, 1964–1995. J. Sound Vib. 190, 495–524.
Mead, D.J., Mallik, A.K., 1976. An approximate method of predicting the response of periodically supported beams subjected to random convected loading. J. Sound Vib. 47, 457–471.
Mead, D.J., Pujara, K.K., 1971. Space-harmonic analysis of periodically supported beams: response to convected random loading. J. Sound Vib. 14, 525–532.
Mead, D.J., Yaman, Y., 1991. The harmonic response of rectangular sandwich plates with multiple stiffening: a flexural wave analysis. J. Sound Vib. 145, 409–428.
Rao, U.N., Mallik, A.K., 1977. Response of finite periodic beams to convected loading—an approximate method. J. Sound Vib. 55, 395–403.
Rumerman, M.L., 1975. Vibration and wave propagation in ribbed plates. J. Acoust. Soc. Am. 57, 370–373.
Ruzzene, M., 2004. Vibration and sound radiation of sandwich beams with honeycomb truss core. J. Sound Vib. 277, 741–763.
Spadoni, A., Ruzzene, M., 2006. Structural and acoustic behavior of chiral truss-core beams. ASME J. Vib. Acoust. 128, 616–626.
Takahashi, D., 1983. Sound radiation from periodically connected double-plate structures. J. Sound Vib. 90, 541–557.
Wang, J., Lu, T.J., Woodhouse, J., Langley, R.S., Evans, J., 2005. Sound transmission through lightweight double-leaf partitions: theoretical modelling. J. Sound Vib. 286, 817–847.
Wang, Y.-Z., Li, F.-M., Kishimoto, K., Wang, Y.-S., Huang, W.-H., 2010. Band gaps of elastic waves in three-dimensional piezoelectric phononic crystals with initial stress. European Journal of Mechanics-A/Solids 29, 182–189.
Wang, Y.Z., Li, F.M., Huang, W.H., Wang, Y.S., 2008. The propagation and localization of Rayleigh waves in disordered piezoelectric phononic crystals. J. Mech. Phys. Solids 56, 1578–1590.
Wang, Y.Z., Li, F.M., Kishimoto, K., Wang, Y.S., Huang, W.H., 2009a. Elastic wave band gaps in magnetoelectroelastic phononic crystals. Wave Motion 46, 47–56.
Wang, Y.Z., Li, F.M., Wang, Y.S., Kishimoto, K., Huang, W.H., 2009b. Tuning of band gaps for a two-dimensional piezoelectric phononic crystal with a rectangular lattice. Acta Mech. Sin. 25, 65–71.
Xin, F.X., Lu, T.J., 2009. Analytical and experimental investigation on transmission loss of clamped double panels: implication of boundary effects. J. Acoust. Soc. Am. 125, 1506–1517.
Xin, F.X., Lu, T.J., submitted for publication. Analytical modeling of wave propagation in orthogonally rib-stiffened sandwich structures: sound radiation. J. Sound Vib.
Xin, F.X., Lu, T.J., in press. Effects of core topology on sound insulation performance of lightweight all-metallic sandwich panels. Mater. Manuf. Processes.
Xin, F.X., Lu, T.J., Chen, C., 2008a. Sound transmission through lightweight all-metallic sandwich panels with corrugated cores. Multi-functional materials and structures, parts 1 and 2 47–50, 57–60.
Xin, F.X., Lu, T.J., Chen, C.Q., 2008b. Vibroacoustic behavior of clamp mounted double-panel partition with enclosure air cavity. J. Acoust. Soc. Am. 124, 3604–3612.
Xin, F.X., Lu, T.J., Chen, C.Q., 2009a. Dynamic response and acoustic radiation of double-leaf metallic panel partition under sound excitation. Comp. Mater. Sci. 46, 728–732.
Xin, F.X., Lu, T.J., Chen, C.Q., 2009b. External mean flow influence on noise transmission through double-leaf aeroelastic plates. AIAA J. 47, 1939–1951.
Xin, F.X., Lu, T.J., Chen, C.Q., 2010. Sound transmission through simply supported finite double-panel partitions with enclosed air cavity. ASME J. Vib. Acoust. 132, 011008:1–011008:11.
Yin, X.W., Gu, X.J., Cui, H.F., Shen, R.Y., 2007. Acoustic radiation from a laminated composite plate reinforced by doubly periodic parallel stiffeners. J. Sound Vib. 306, 877–889.